POLITECNICO DI TORINO

Master’s Degree in Mechatronic Engineering

Master’s Degree Thesis

Modelling and Control of Alternative Hybrid Propulsion Systems for High Efficiency Passenger and Heavy-Duty Vehicles

Supervisor:

Prof. Angelo Bonfitto

Co-supervisor:

PhD candidate Saulius Pakštys

Candidate:

Gianmarco D’Emilio

April 2024

Abstract

As the global pursuit of sustainable mobility/transportation intensifies, the need for reducing emissions from conventional vehicles becomes crucial. This thesis addresses this imperative by exploring the integration of advanced energy storage and conversion systems within the framework of Energy Management System (EMS) for electric bus. In recent years, research in Hydrogen Fuel Cell as a source of energy has been growing more and more, especially for heavy transport vehicles such as city buses, and, in particular, coupled with batteries or supercapacitors to eliminate the problem of their slow dynamic response.

This thesis is produced to describe, model, and simulate an alternative hybrid powertrain for city bus in order to maximize overall energy efficiency. For this purpose, key performance indicators, including energy efficiency and battery c-rate are evaluated under different operating conditions such as payload and driving cycles.

In the initial section, a state-of-the-art analysis of the available technologies about Electric Vehicles is performed, starting from traditional ones (ICE-based) to vehicles with different energy storage technologies (Hybrid Electric Storage System, HESS) . It examines the main methodologies and architectures, showing the advantages and disadvantages of each.

In the following, a pure electric bus is considered, where the powertrain is supplied by the combination of battery system and a supercapacitor (SC) pack, introduced to the system, in parallel to the battery allowing to fulfill the bus's overall power request reducing the stress experienced by the battery.
A comparative analysis is carried out between different control strategies, starting from a rule-based controller (RBC) , which is later improved to adapt to different drive cycles (A-RBC) . Finally, a Fuzzy logic controller based is used.
The results obtained show a decrease in the C-rate experienced by the battery, with a value of Root Mean Square that is 32.1% lower than the one obtained without the use of SC, which is corresponding to an extension of battery life.

In the second part, a vehicle model based on fuel cell is described, which operates in charge sustaining mode and uses a smaller battery than that of the normal production vehicle (-83,3%). Two different control techniques, namely a rule based and a fuzzy logic, are explored for the HESS management, to improve efficiency.
Finally, SC pack is introduced to support the battery as a power buffer, significantly reducing the stress to which it is subjected. This configuration allows limiting the C-rate experienced by the battery to a maximum acceptable value of less than 2C, reducing the total mass of the energy storage system by 1200 kg (-69%) with respect to the normal production vehicle battery.

In conclusion the main findings of this activities are:

- In the powertrain configuration equipped with Battery and SC pack, 32,1% reduction in battery C-rate is achieved.

- In the powertrain configuration equipped with Battery, Fuel cell and SC pack, the total mass of the HESS is reduced by 1200kg (-69%), while maintaining the C-rate limited to a maximum value of less than 2C.

The study highlights the significance of optimal energy management in addressing the challenge of improving the sustainability of electric buses and contribute valuable knowledge to the field of electric vehicle, offering a nuanced understanding of the synergies between different energy storage technologies in the pursuit of greener and more efficient urban transportation.

Acknowledgements

I would like to thank my academic advisor, Professor Angelo Bonfitto for the opportunity he gave me to write this thesis and explore this field of research. A huge thank you goes to Saulius Pakštys for the continuous support, availability and advice he has given me during these months.

Thanks to my family: my parents, who have always supported me in my life choices, can never be thanked enough. My brothers who have always been a source of inspiration for me and thanks to whom I have become the person I am, I love you so much.

To my girlfriend wonderful Chiara, I thank you for always being patient with me, for loving me as I am and for not judging me. I know it can't be easy and that's why your support is even more appreciated.

Finally I want to thank all my friends who have been close to me during these years and these last months, Francesco and Andrea and Roberto, for your closeness even when many kilometers separated us. To the people I found here and who were the best second family I could wish for, Ema, Novi, Squalo, Giovanni and Nico and all the others. Finally, I want to thank Arash, Orazio and Angelo, without joking with you during these months it would have been much more difficult

Table of contents

List of Tables

List of Figures

INTRODUCTION

Climate change challenges

"We are living on this planet as if we had another one to go to" [1]. The growing awareness of climate change and global warming has brought into focus the need to adopt sustainable practices in various sectors of our society. One of the critical aspects that contributes significantly to the increase in greenhouse gas (GHG) emissions is represented by the transport sector, responsible for around a quarter of total CO_2 emissions in Europe, 71.7% of which is produced by road transport [2]. Dependence on fossil fuels for personal and commercial mobility has generated a number of negative environmental impacts, contributing to ongoing climate change. In recent years, the implementation of regulations aimed at reducing emissions and promoting sustainability in the transportation sector has triggered significant mobilization by Original Equipment Manufacturers (OEMs). These regulations, such as “Fit for 55”[2] or the European Green Deal [3], have imposed tighter restrictions on emissions of greenhouse gases and air pollutants, prompting the automotive industry to invest heavily in research and development of alternatives to traditional internal combustion engines. In this context, OEMs have understood that the adoption of sustainable practices and technologies not only responds to current regulations, but also reflects a growing consumer demand for greener vehicles [4].

Alternative to traditional combustion engine vehicles

Hybrid Electric Vehicles

Hybrid vehicles are so named because they feature propulsion systems with two complementary energy sources: a high-capacity storage (usually a chemical fuel in liquid or gaseous form) and a lower-capacity rechargeable energy storage system (RESS)[5]. The RESS not only acts as an energy storage buffer but also enables the recuperation of vehicle kinetic energy and provides power assistance. Electrochemical (batteries or supercapacitors), hydraulic/pneumatic (accumulators), or mechanical (flywheel) systems can serve as the RESS.

The most widespread are hybrid electric vehicles (HEV), which use electrochemical batteries such as RESS, and electric machine (EMs) as secondary energy converters, while the internal combustion engine (ICE) is the primary energy converter, powered by traditional fuel; however, fuel cells or other types of combustion engines can be the primary energy converter [6].

It is possible to classify HEVs based on the size of the internal combustion engine and electric machines, i.e. based on the degree of hybridization, as shown in Figure 1:

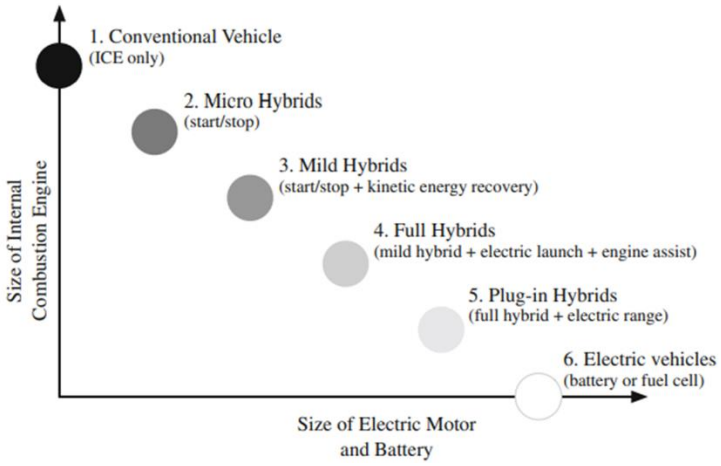

***Figure 1**: Degrees of hybridization of an HEV, starting from a traditional vehicle with ICE up to totally electric vehicles*

The principal characteristics of different types are summarized below:

- conventional vehicles: vehicles powered only by the ICE.
- in micro hybrid vehicles a start-stop system allows to automatically shut off the ICE when the vehicle is stationary. This helps reduce fuel consumption and emissions during idling.
- in a mild hybrid vehicle, a small electric machine and a low-voltage battery assist the internal combustion engine. Unlike full hybrids or plug-in hybrids, mild hybrids do not have the capability for extended electric-only propulsion. Instead, they use the electric components to enhance the efficiency of the ICE.

It offers some of the benefits of hybridization, like regenerative braking systems or limited electric assist, without the need for large and expensive battery packs.

- full hybrid electric vehicles (FHEV), due to the high-capacity battery, have the capability for significant electric-only driving. The two power sources can operate independently or in conjunction, depending on driving conditions and energy demands. At this level of hybridization, more complex energy management strategies are needed to fully exploit the characteristics of the vehicle.
- in Plug-in hybrid electric vehicles (PHEV), rechargeable batteries that can be restored to full charge by connecting them to an external electric power source are used to extend the range.
- electric vehicles (EV) are powered only by electric motor(s), which use as primary source of energy electricity stored in batteries or a hydrogen fuel cell.

HEVs architectures

The position and the number of electric machines define the architecture of the HEV, that can be classified as follows:

- series: the ICE drives a generator that produces electrical power, which is summed to the power coming from the RESS and is used by the EMs. The main advantage of this configuration is the need of only electrical connections between the power conversion devices. Furthermore, since the engine is completely separated from the wheels, there is freedom to choose the load and speed, thus operating at the maximum possible efficiency. However, the main drawback is represented by the fact that this configuration requires two energy conversions, from mechanical to electrical in the generator and from electrical to mechanical in the EM, introducing large losses [7].
- parallel: ICE and EMs are connected in parallel. In this case the power summation is mechanical rather than electrical: the power from EMs and ICE are pooled together with the help of mechanical coupling, so that their torque is summed and then transmitted to the wheels. There's no freedom for choosing the speed of the engine because it's mechanically related to the wheel speed. On the other hand, the elimination of the generator reduces the losses and weight of the powertrain [8].
- power split and series parallel: these architectures combine series and parallel operation and advantages, by connecting EMs and engine to a power split device like a planetary gear set (power split) [9]. In the series parallel architecture, the engagement/disengagement of clutches allows to change the configuration from series to parallel [10]. Both allow for greater flexibility and control but using double convection only for a part of the total energy, decreasing the associated losses.

Battery Electric Vehicle

The most common fully electric vehicles are the Battery Electric Vehicles (BEV), which use as energy storage system high voltage electrochemical batteries. The energy stored in batteries is used to drive one or more electric motors [11]. These vehicles produce zero tailpipe emissions during their usage and, in regions with a significant share of renewable energy in their electricity grids, BEVs can result in lower overall GHG emissions compared to traditional vehicles. The main disadvantages of BEVs are the limited driving range on a single charge with respect to a traditional combustion engine car, and the large size and mass of the battery to meet the power demands of the vehicle, avoiding operating currents (and C-rates) that are too high, which would lead to rapid degradation of the battery [12]. Furthermore, another important aspect to consider is the environmental impact due to the production and disposal of batteries, which represents a large part of the total emissions of a BEV [13].

Many different types of batteries are on the market, such as Lithium-Ion Batteries or Nickel-Metal Hydride Batteries [14]. In this thesis a vehicle using lithium-iron-phosphate ($LiFePO_4$ or LFP) batteries will be analyzed. In recent years LFP batteries have had a great diffusion, mainly due to Chinese OEMs. More than 95% of heavy-duty vehicles produced in China are equipped with LFP batteries, which, due to their durability and lower price, are the best choice to meet the mileage needs of these vehicles [15]. The reason behind their economic convenience lies in the fact that these batteries are made with relatively cheap metals (iron and phosphorus) compared to those used in other batteries such as nickel, cobalt and manganese.

Fuel Cell Hybrid Electric Vehicle

Another mobility solution that does not emit GHG is represented by Fuel Cell Electric Vehicles (FCEV). For this reason, in recent years several OEMs have presented vehicles based on this technology

Fuel Cell Electric Vehicles using hydrogen as an energy source, which is utilized inside the fuel cell to produce usable electrical energy. In Fuel Cell Hybrid Electric Vehicles (FCHEV) accumulation and recovery of energy during braking or periods of low energy demand is possible through the incorporation of a smaller battery pack or supercapacitor. The most common type of fuel cell is the Proton Exchange Membrane Fuel Cell (PEMFC): after splitting the hydrogen into its components, proton (H^+) and electrons (e^-), protons pass through the membrane, while electrons are unable to cross it and following an alternative path known as an external circuit, they provide electrical energy by passing through an electrical load. Finally, the positive H^+ ions react with the oxygen present in the air forming H_2O [16].
The complete reaction is as follows:

$$2H_2 + O_2 \rightarrow 2H_2O + energy$$

The entire process produces water as the only by-product, highlighting how fuel cells are able to efficiently generate zero-emission electricity. However, it is necessary to remember that the production of hydrogen is associated with the emission of a certain quantity of GHG, even if methods for obtaining hydrogen in a clean way have been developed and are becoming widespread [17]. The biggest obstacle to the use of fuel cells for alternative powertrains is represented by their low dynamics and power density characteristics. Fuel cell suffers from a slow dynamic response and is difficult to adapt to complex driving conditions. For this reason, they are often used in hybrid energy storage systems with a battery.

Supercapacitors in Hydrid Electric Vehicles

As has already been illustrated in the previous paragraphs, unless the battery system is oversized, it may experience excessively high C-rates due to the high peak power requirements, thus undergoing faster degradation. An excellent solution is to use a supercapacitor (SC) as a power buffer, to achieve overall better performance in terms of battery C-rate. Compared to batteries, SCs have a higher power density and a life, expressed in terms of charging cycles, up to 1000 times longer. On the other hand, the lower energy density makes it necessary to use together with a battery system [18] [19]. By coordinating effectively, the battery will provide the necessary energy from the powertrain, while the SC will handle the high-power demands. There are different configurations to connect the battery and the SC [20]:

- basic passive configuration: the battery and the SC are directly connected in parallel without converter/inverters. It is the simplest and most easily implementable configuration; it does not require control systems or power electronics converters. However, it does not use the SC efficiently as its voltage must be the same as that of the battery, not allowing the energy stored within it to be fully used.
- semi-active configuration: by using a bidirectional DC/DC converter to interface the SC, it's possible to fully exploit the stored energy. This configuration requires expensive and heavy converter and more complex control techniques.
- fully active: to allow for a wider operating range and higher utilization of the stored energy of the UC, another bidirectional DC/DC converter was added between the UC bank and the DC link, allowing to control the system in best and most complex way. However, this solution turns out to be more expensive and heavier, due to the presence of the additional DC/DC converter [21].

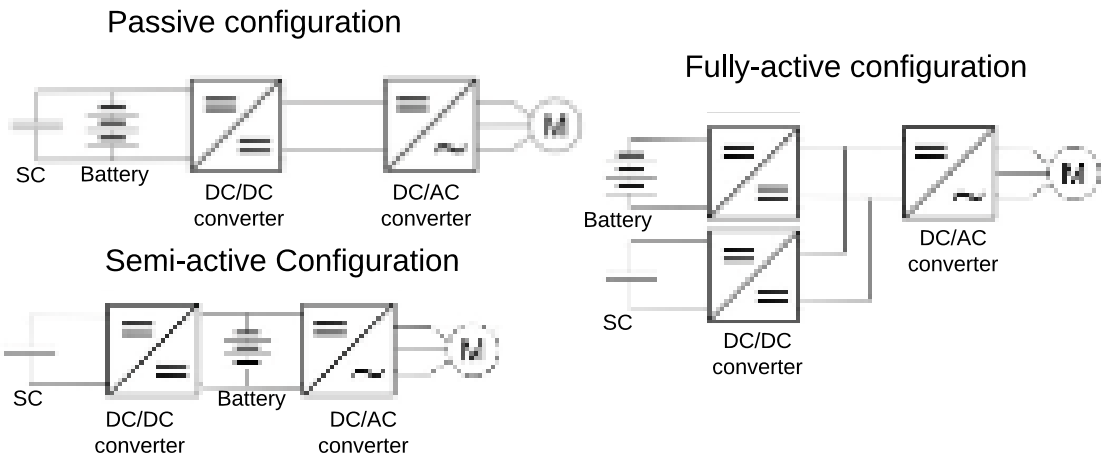

***Figure 2**: Battery and Supercapacitor possible configurations*

Energy Management Strategies

Energy management in HEV concerns in deciding the amount of power delivered at each instant by the energy sources of the vehicle while meeting several constraints [22]. This is a crucial operation, as it leads to a more efficient use of the vehicle's energy, reducing consumption, costs, and emissions.

Two sets of tasks are executed to control a HEV: a low-level or component-level control task, where, through feedback control methods, each component of the powertrain is controlled, and a high-level or supervisory control. The latter, which deals with optimizing energy flows inside the vehicle, is called Energy Management System.
EMS receives information from the driver and the vehicle, processes it and outputs an optimal set of commands to be executed by the actuator, controlled by the low-level control layer. There are several methods to determine the optimal power split between the different energy sources present in an HEV [23].

The EMS can be categorized into several types, each with its own set of advantages and disadvantages (Figure 3). Among these, the two most commonly used strategies are rule-based and optimization-based approaches.

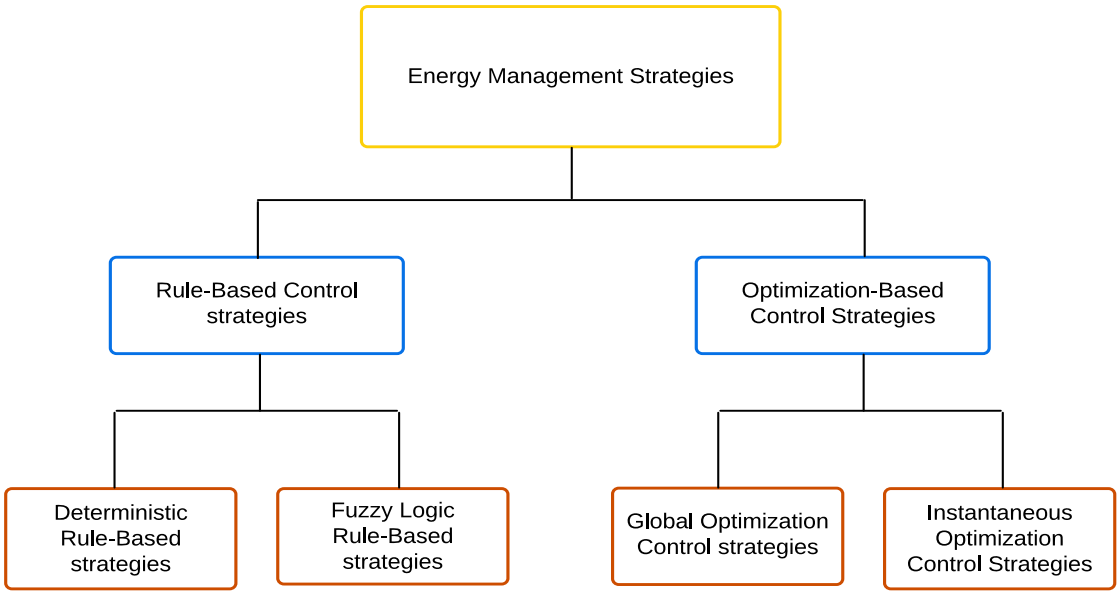

***Figure 3**: Control strategies for HEV scheme*

Rule Based Control Strategy

A rule-based control is a deterministic energy management strategy. Its main feature is its effectiveness in real time application. It relies on a set of rules, predetermined based on heuristics or on optimal solutions obtained through mathematical models [22]. RBC is a fast and computationally efficient method, but it can fail to provide the optimal solution, since it does not implement optimizations. Furthermore, it requires extensive knowledge of the system under examination. In the literature it is widely used as a basis for EMS of HEV [24], and in this thesis it is implemented and compared with other methods.

Fuzzy Control Strategy

Fuzzy logic can be used to perform energy management strategy. The term Fuzzy logic was introduced in 1965 by Iranian mathematician Lofti Zadeh and indicates a many-valued logic in which each proposition can be attributed a degree of truth different from 0 and 1 and included between them [25]. Fuzzy Logic Controllers (FLC) are particularly suitable for EMS in HEVs because they can handle the uncertainty and imprecision associated with real-world driving conditions. Using Fuzzy inference system, it's possible to formulate the relationship between a provided input to an output using fuzzy logic [26]. Fuzzy inference is a method that analyzes the values in the input vector and based on some sets of rules, assigns values to the output vector and is composed by:

- input variables: such as driving conditions, driver inputs or battery State of Charge (SOC).

- rules: a set of If-Then rules that define the relationship between input variables and the control actions. Rules are formulated based on knowledge and experience, or through a learning process.
- membership functions: fuzzy logic uses membership functions to represent the degree of membership of a variable in a fuzzy set.
- inference engine: The inference engine evaluates the rules based on the current input values and determines the degree to which each rule is satisfied.
- output variables: in the case of an FLC that deals with EMS, the output usually indicates the division of the power required from the different energy sources
- defuzzification: is the process that convert the fuzzy output, described in terms of membership in fuzzy sets, into a quantifiable result in crisp logic. There are several methods for defuzzification, like Center of Gravity or Centroid method [27], [28] .

The main advantages of FLG are the ability to adapt to varying and uncertain conditions, the easy implementation compared to complex mathematical models, the transparency in the decision-making process and the tuning flexibility.

Dynamic Programming

Another strategy that can be used is the dynamic programming (DP), a numerical methodology that, by working backward in time, identifies the globally optimal solution [29]. First, progressively longer tail sub-problems are solved iteratively, and the global cost for each iteration, along with potential state variables, is stored. After that, the optimal sequence of controls is found by choosing the one which, starting from the initial state, minimizes the global cost function. DP can offer the optimal solution for problems of any complexity level, but nevertheless, it is noncausal and can only be implemented in a simulation environment due to its dependence on a priori information about the entire optimization horizon.
For these reasons, it is often used as a benchmark, comparing its results with other control strategies to assess their efficiency [29].

Other control techniques are examined in the literature for the energy management problem, such as Equivalent Consumption Minimization Strategy (ECMS) [30], Pontryagin's Maximum Principle (PMP) [31], or Model Predictive Control (MPC) [32].

Thesis objectives

The first objective is to increase the lifespan of the battery in a city bus through the introduction of a supercapacitor pack. To achieve this, the experienced battery C-rates, will be considered as a key performance indicator. Additionally, various control techniques for the Energy Management System will be implemented. Measuring the actual increase in battery lifespan is a very complex challenge. However, through quantitative measurement indicating the decrease in C-rates, it is possible to arrive at a qualitative conclusion about the increase in battery life.
The second objective is to size and reduce the total mass of a Fuel Cell-based Hybrid Electric System operating in charge-sustaining mode by significantly diminishing the battery size. Lastly, the benefits obtained by introducing a supercapacitor pack working in synergy with the battery, thereby reducing the stress on the battery, will be emphasized.

In the first part of the thesis, the model of the BEV bus under study will be presented, with particular focus on the modeling of the power sources used, namely the battery and the SC pack introduced to assist the battery and extend its life. After selecting the appropriate configuration, three energy management strategies, a Rule Based Controller, an Adaptive-RBC and a Fuzzy Logic Controller, will be presented and compared using the experienced battery C-rate value as KPI. The simulations will be conducted in the MATLAB & Simulink environment, utilizing various drive cycles and vehicle masses to simulate different driving scenarios.

In the second part of the thesis, the model of an FCHEV will be presented, developed with the aim of reducing the mass of the HESS, and its performance will be compared with that of the BEV baseline bus. Again, two control strategies will be explored, one being a rule-based strategy and the other based on fuzzy logic. Finally, the impact of an SC pack on the FCHEV in terms of C-rate reduction will be evaluated.

I SECTION: Battery and Supercapacitor Hybrid Electric Storage System

Battery and Supercapacitor pack Hybrid Electric Storage System modelling

The first part of this thesis focuses on the analysis of an urban Battery Electric Vehicle and the introduction of a Supercapacitor pack. To study this configuration, a vehicle model has been implemented in the MATLAB & Simulink environment.

Vehicle model

The studied vehicle is the BYD K9 series 12-meter-long eBUS [34], which is taken to be the baseline vehicle. Table 1 outlines its main characteristics.

Dimension/Weight			
Characteristic	**Notation**	**Unit**	**Value**
Length/Width/Height	L/W/H	m	12.05/2.55/3.36
Mass	M	kg	13000
Gross Curb Weight	GCW	kg	16000
Wheelbase	L	m	5.9
Height of CG	hG	m	0.5
Frontal area	A_f	m^2	8.568
Drag coefficient	C_d	-	0.5
Tire inertia	I_t	$kg*m^2$	0.8
Rolling radius	r	m	0.49
Powertrain			
Characteristic	**Notation**	**Unit**	**Value**
Maximum Power	P_{max}	kW	300 (2x150)
Maximum Torque	T_{max}	Nm	1100 (2*550)
Battery			
Type	Lithium-Iron Phosphate LFP		
Rated Operational Voltage	V		540
Energy	kWh		324
Capacity	Ah		600

***Table 1**: Vehicle Characteristics*

In this thesis, the adopted model was implemented relying on a forward scheme, that was preferred over the backward scheme because it is well-suited for modeling intricate dynamics. (Figure 4)

In the backward scheme, a target speed is specified by a driving cycle. The required propulsive force is calculated using Newton's second law and then, along with the vehicle speed, is propagated through the powertrain. The input power necessary for the propulsion effort is subsequently computed.
In the forward scheme, a target speed is also supplied by a driving cycle, but it undergoes a driver model. The driver governs the longitudinal vehicle interfaces, specifically the accelerator and brake pedals, by considering the disparity between the target speed and the current vehicle speed. The torque is then propagated forward through the powertrain to the wheels. Newton's second law determines the vehicle acceleration, which is integrated to derive speed and position. The position is fed back to the driving cycle to determine a new target speed, completing the computation loop [33].

The requirement for a driver model to control the vehicle interfaces in the forward method makes it conceptually closer to real-world situations compared to a corresponding backward method, but it adds complexity to the model.

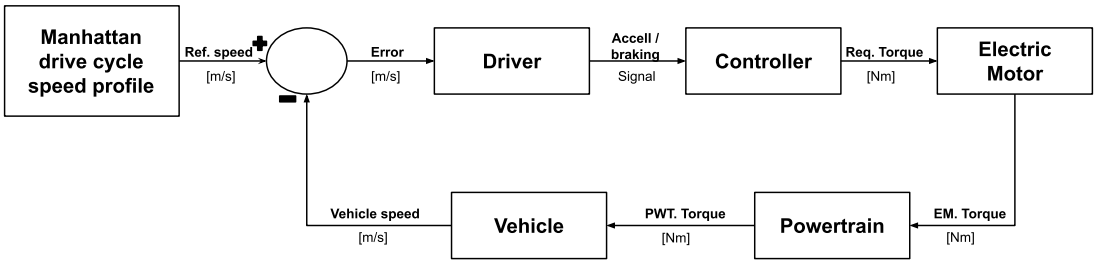

***Figure 4**: Forward architecture block scheme*

The model implemented in Simulink consists of two main subsystems: the controller and the plant, which are connected by their respective inputs and outputs as shown in Figure 5:

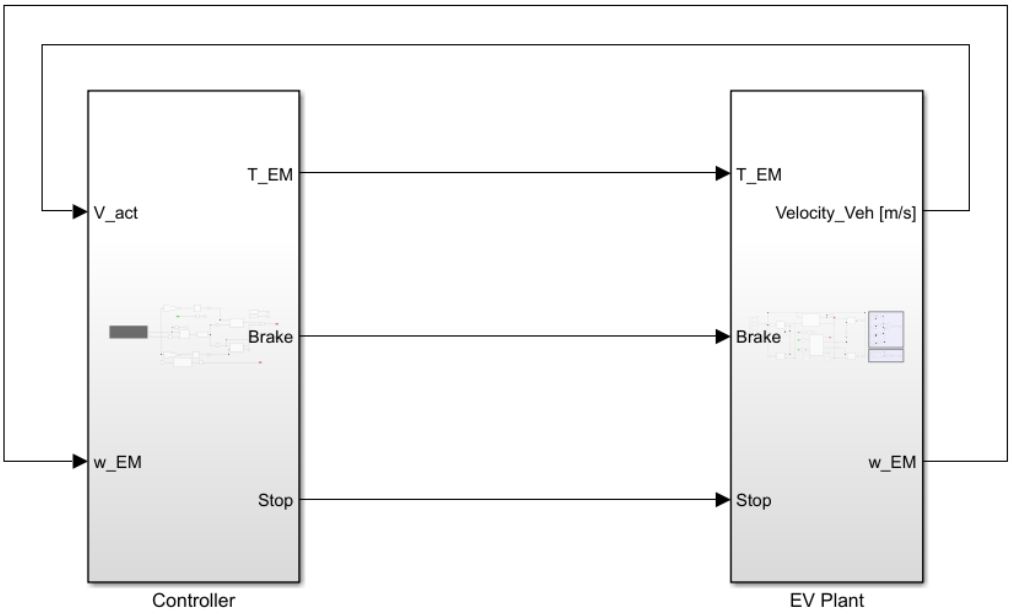

***Figure 5**: Controller and Plant subsystem structure in Simulink*

The controller, shown in Figure 6, generates the speed profile using the loaded drive cycle as reference. The error is calculated as the difference between the reference speed and the current speed of the vehicle, and this error is translated by a Proportional-Integral (PI) controller into a normalized signal for acceleration or braking. The output of the PI controller is translated into a signal indicating the torque required for the Electric Machine (EM), which is then compared with the limit value it can assume based on the current operating point and, if necessary, saturated before being sent to the plant, along with the brake signal.

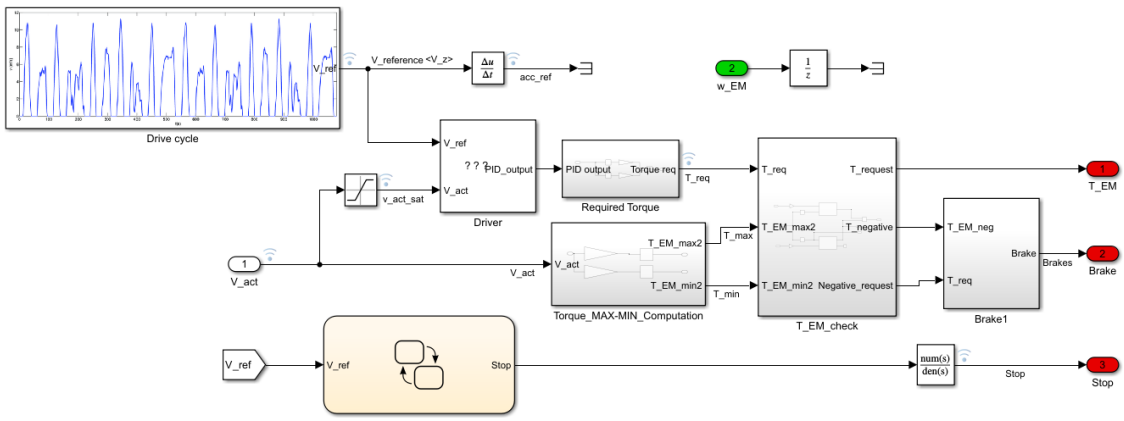

***Figure 6**: Controller subsystem structure*

For the generation of the driving cycle, real speed and position data collected from a bus operating on the streets of Manhattan were used. The resulting driving cycle, characterized by frequent stops has been utilized in literature for the homologation of city buses [34]. Their characteristics are summarised in Table 2:

Parameter	Unit	Value
Total cycle time	s	1089
Maximum speed	m/s	11.24
Average speed	m/s	3.03
Maximum acceleration	m/s^2	2.04
Covered distance	m	3300

***Table 2**: Manhattan drive cycle parameters*

In the plant, the model for vehicle longitudinal dynamics is present. It's a Simulink block closely interacting with the tire model, determining forces applied to each of the four tires, as well as controlling vehicle speed and horizontal movement. The plant also includes models for the two EMs and power sources (Figure 7).

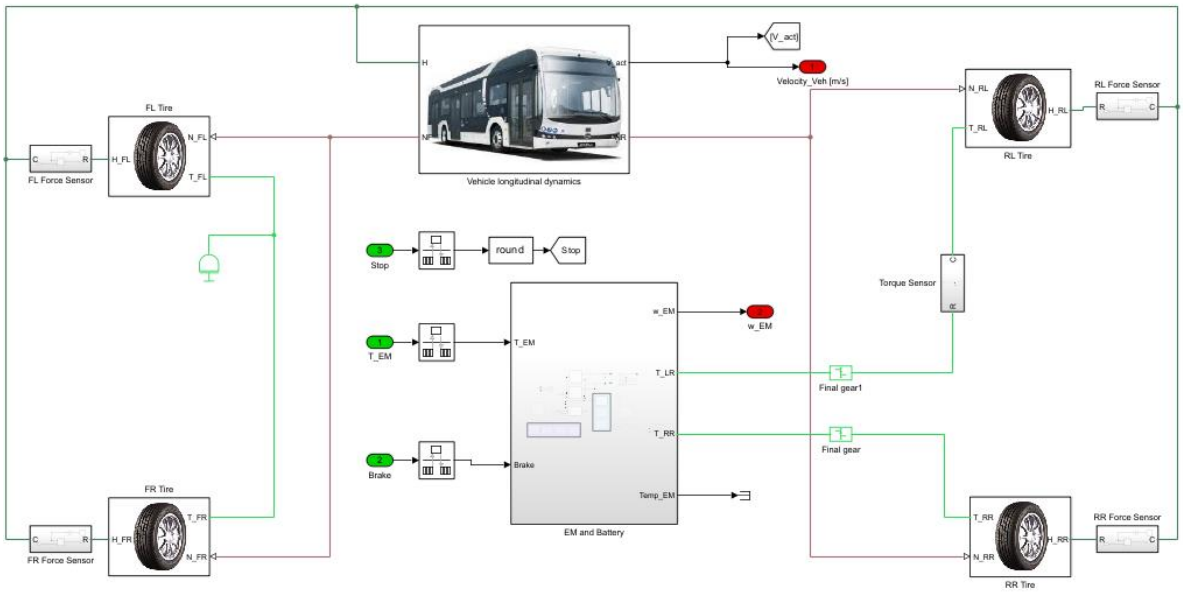

***Figure 7**: Plant model structure in Simulink*

In the vehicle, two identical EMs are present, and each one of them has been modeled using a look-up table based on torque-speed map of a electric motor, appropriately modified using scaling factors to fit the characteristics of the electric machines present in BYD bus. In Figure 8 the scaled Torque-Speed map is presented.

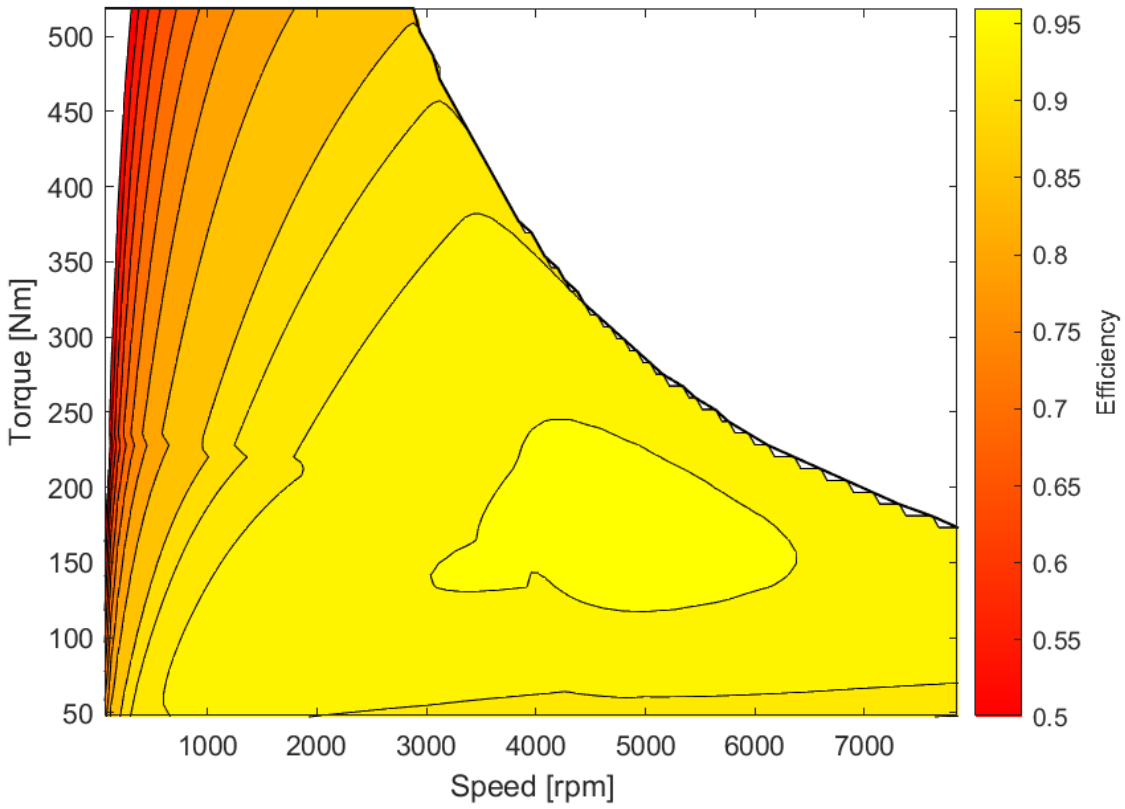

***Figure 8**: Torque-Speed map of one EM*

The fourth quadrant of this map appears specular to the first, and for this reason, it has been omitted. The model of the EM generates a power request based on this map, which is met by the available power sources, as will be described in detail later.

Power sources modeling

In this section, the analysis will focus on the models of power sources, namely the battery and supercapacitor, presented in Figure 9.

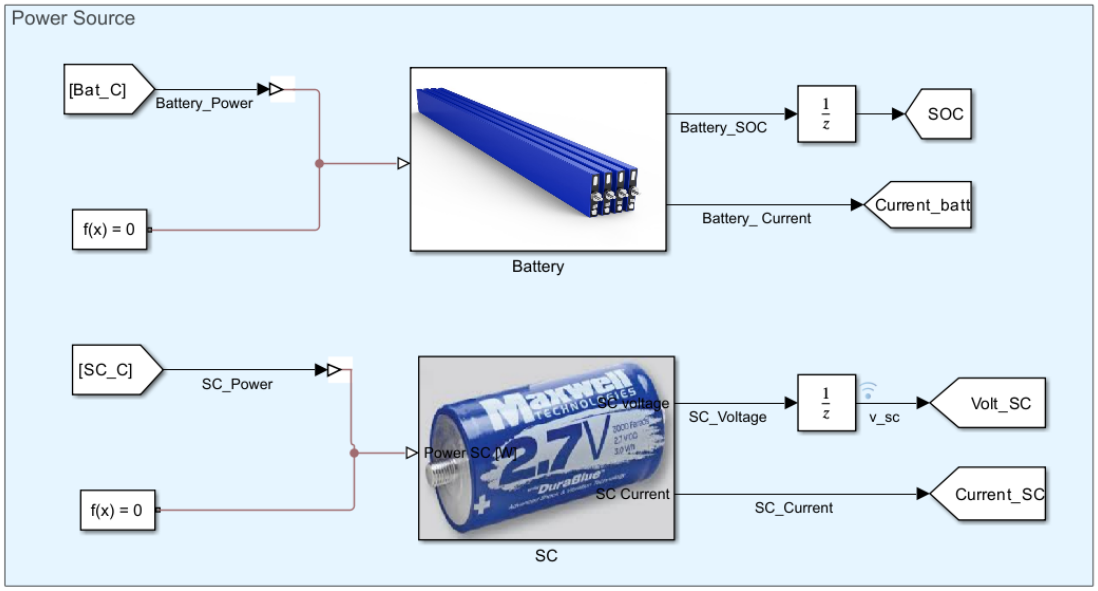

***Figure 9**: Power sources model in Simulink*

Architecture

The introduction of a supercapacitor pack alongside the battery as a power source implies a study of possible configurations to choose the most advantageous one.
As mentioned in the introduction, the various configurations in which the battery and supercapacitor work in parallel differ from each other in terms of the relative position of the two energy sources, as well as the presence of one or more DC/DC converters. Among the various configurations, the semi-passive one has been chosen for this thesis, which involves the use of a bidirectional DC/DC converter placed between the supercapacitor pack and the battery. In this way, it is possible to make the most of the supercapacitor, as it is necessary to allow the voltage to vary for effective utilization. The disadvantage incurred by using this component, however, is due to its high cost, the additional mass introduced into the system, and power losses. A scheme of this configuration is reported in Figure 10:

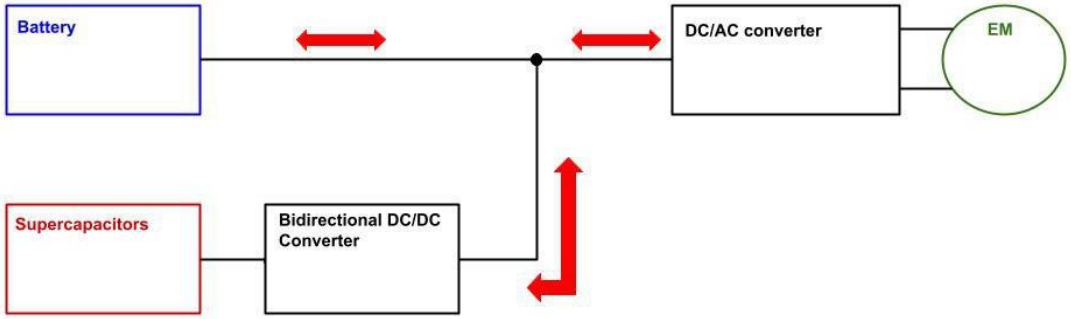

***Figure 10**: Semi-active architecture*

In this work, the decision has been made to refrain from modeling DC/DC converters, as the main focus is to explore control strategies for energy management and analyze the impact they can have, rather than the physical representation of individual components.

Battery

The main characteristics of the battery used in the BYD electric bus model K9-12 meters are reported in Table 3. The entire battery pack is composed of numerous cells arranged in series and parallel to achieve the required capacity and voltage. A cell manufactured by BYD for the automotive industry, BCT 200Ah, was chosen to adequately meet the capacity and voltage requirements of the vehicle. The characteristics of this cell are provided below.

Parameter	Unit	Value
Chemistry	-	Lithium-Iron Phosphate
Type of cell	-	Prismatic
Rated capacity	Ah	200
Rated voltage	V	3.2
Weight	kg	3.43
Size	Mm	390x140x60
Working temperature	°C	20– 60
Cycle life	-	2000 discharge cycles (< 1C)

***Table 3**: Battery cell parameters*

The number of cells required to be connected in series and in parallel to form the battery pack is determined through simple calculations based on the specifications provided in the vehicle's datasheet. To calculate the number of cells in series, the total voltage is divided by the voltage of a single cell, and for the number of cells in parallel, the total capacity of the battery is divided by the capacity of a single cell. This results in 169 cells in series and 3 cells in parallel.
The overall mass of the battery can now be easily calculated and is equal to 1740 kg.
The battery is represented as an ideal voltage source. Its Simulink model has not been explored within the scope of this thesis but has been obtained from prior research conducted at the DIMEAS (Dipartimento Ingegneria Meccanica e Aerospaziale) of Politecnico di Torino. Figure 11 illustrates how the battery is represented in Simulink.

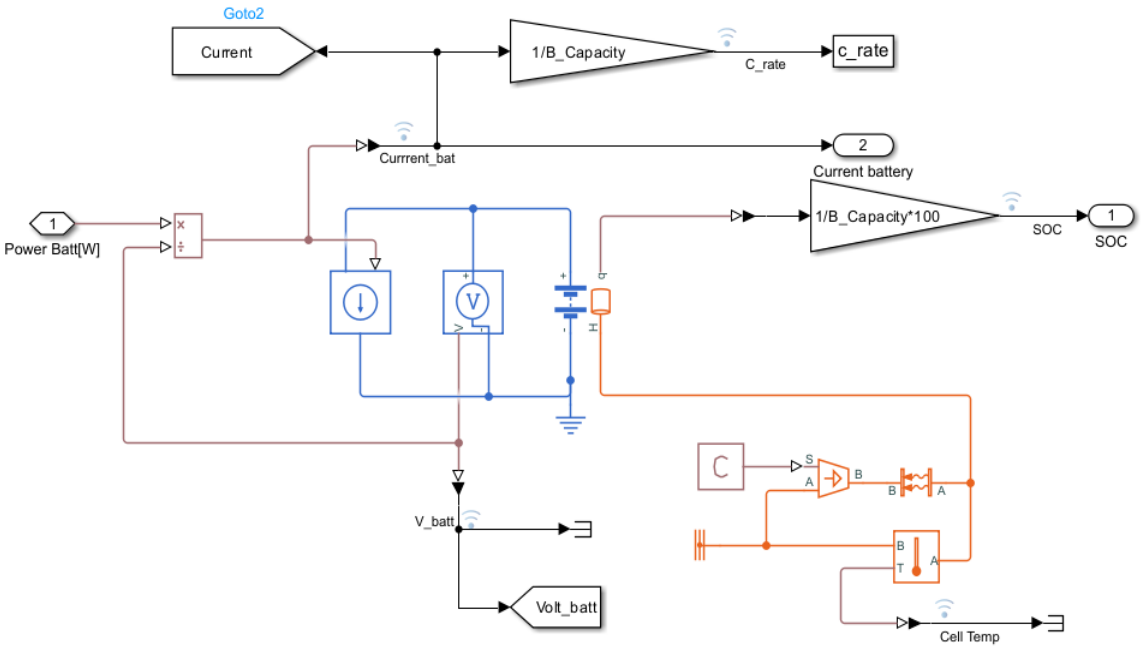

***Figure 11**: Battery model in Simulink*

Supercapacitor

For the supercapacitor pack, the choice fell on the BCAP3000 P270 K04/05 supercapacitor cell manufactured by Maxwell. Its characteristics are presented in Table 4.

Parameter	Unit	Value
Rated capacitance	F	3000
Max. rated capacitance	F	3600
Rated voltage	V	2.7
Peak current	A	2300
Continuous current	A	280
Weight	kg	0.475

***Table 4**: Supercapacitor cell parameters*

This specific SC cell has been chosen for its high-power characteristics and its typical applications in the heavy transport sector. In this case, the decision was made to achieve a voltage on the supercapacitor (SC) pack equal to that of the battery (540 V). To reach this, 200 cells are connected in series, while only one row of cells is used in parallel. The total mass of the SC pack is thus 95 kg.

The representation of a supercapacitor has been accomplished using various types of equivalent circuit models. The equivalent circuit model of a supercapacitor includes fundamental electrical components, such as a resistor and a capacitor. These components may exist as a singular unit or multiple units connected either in series or parallel configurations. Among the most common, there are the Stern-Tafel model [35], the Zubieta model [36] and the series model [37]. In this work, the Zubieta model has been chosen, as it is a highly accurate yet simple. The Zubieta model used in this thesis comprises a circuit featuring three parallel RC time constants with fixed resistances and capacities and it's shown in Figure 12. The initial branch, with elements R_0C_0 and the voltage-dependent k_cv_c, delineates the response in seconds. The second branch, R_1C_1, contributes to the response in the minute range. The R_2C_2 branch characterizes the response for durations longer than minutes. Lastly, a resistor R_{lk} simulates the leakage resistance.

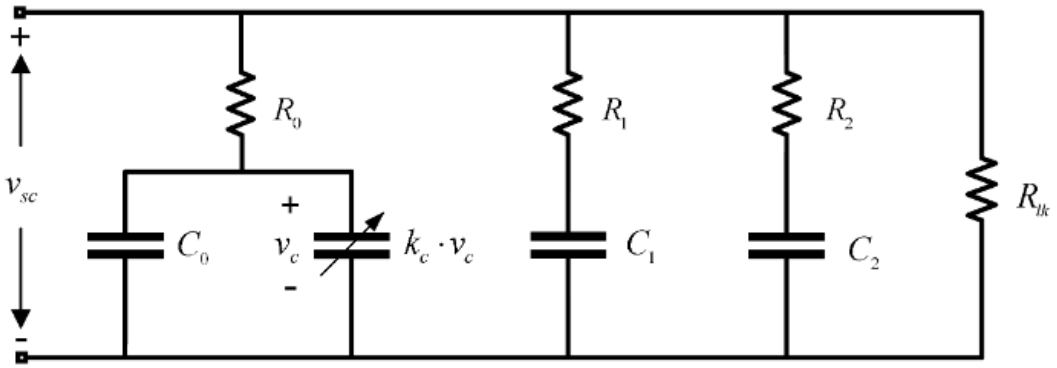

***Figure 12**: Electric circuit of the Zubieta model*

The features of the selected supercapacitor cell have been established through experiments conducted by [38] and have been incorporated into this study. They are outlined in Table 5.

Parameter	Notation	Unit	Value
Fixed resistances	R_0	Ω	0.322e-3
	R_1		0.38065
	R_2		1.3284
Fixed capacities	C_0	F	2934.7
	C_1		76.841
	C_2		1518.8
Voltage-dependent gain	k_c	F/V	130.81
Leakage resistance	R_{lk}	Ω	59436

***Table 5**: Zubieta circuit parameters for SC cell*

In Figure 13, the model implemented in Simulink is shown.

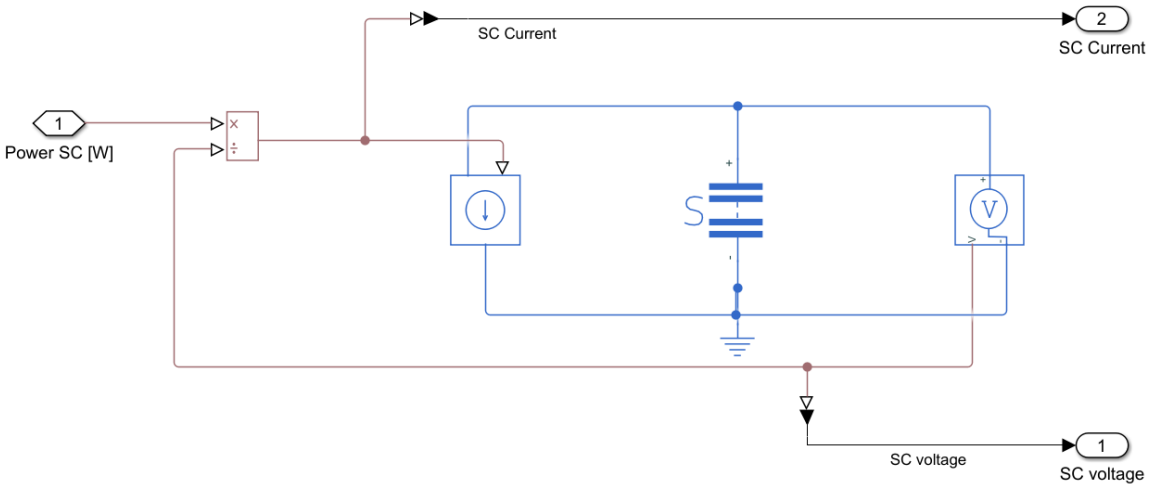

***Figure 13**: Supercapacitor model in Simulink*

Control techniques

The first part of this manuscript explores the benefits derived from introducing an SC pack that complements the battery as a power source. To achieve this, various EMSs will be studied, and their results will be compared with each other and with those obtained from the vehicle equipped only with the battery.

In the case of a Battery Electric Vehicle, an energy management strategy may not be necessary since all the power required at each moment is supplied directly by the battery, the sole power source. However, in the case of a Hybrid Energy Storage System, it becomes crucial to decide appropriately how much power should be dispatched at each moment from the available power sources.

For the SC to be utilized effectively, it needs to be engaged during periods of peak power demand. This intervention is crucial to reduce the stress that would otherwise be imposed on the battery. Nevertheless, due to its lower energy density, it is crucial

to utilize the supercapacitor only when absolutely necessary. This is done to prevent its voltage from decreasing too much, ensuring that the energy stored within it is not excessively consumed.

Rule Based Control

The initial approach to the energy management strategy for the Hybrid Electric Storage System is to formulate a rule-based control strategy. This strategy aims to calculate the optimal power distribution between the SC pack and the battery.
The logic of the algorithm is presented in Figure 14.

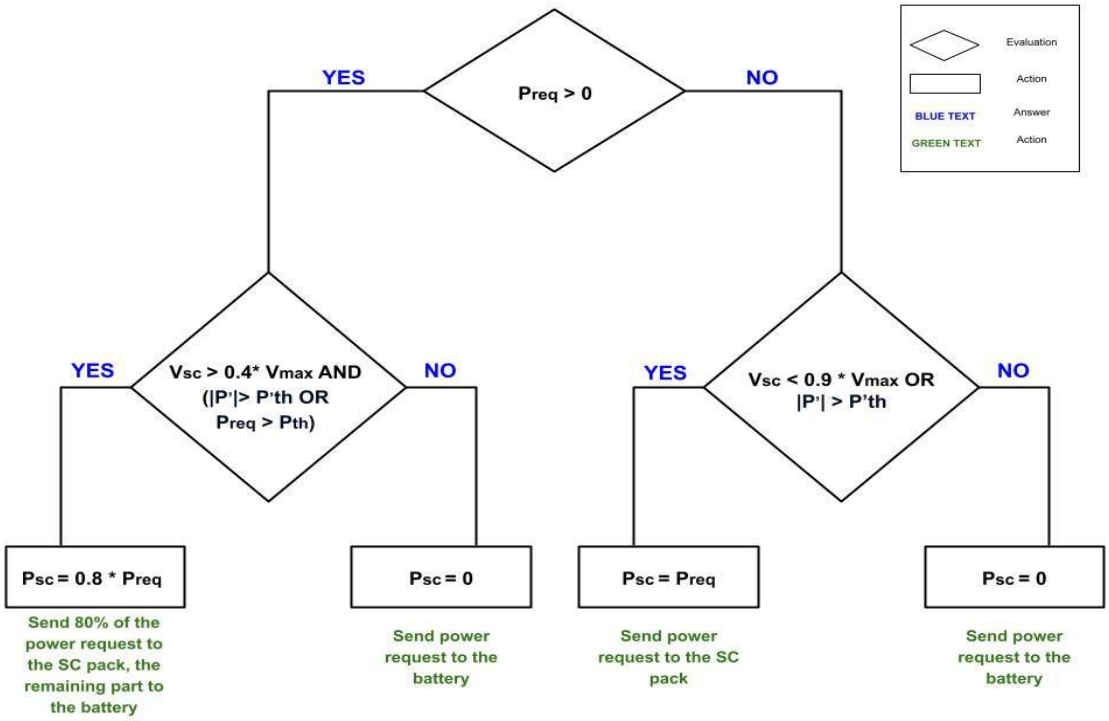

***Figure 14**: Flow chart of the RBC*

The Rule Based Controller is implemented in Simulink through a MATLAB function block. This controller determines the powers required by the SC pack and the battery based on predefined control rules and using thresholds for vehicle parameters. In particular, three parameters are considered: the power demand from the EM, the time derivative of this power, and the voltage of the SC.

- The power demand is considered to ensure that the Supercapacitor pack limits the battery current and thus reduces the maximum C-rate values.
- The power derivative is used as a parameter by the Rule-Based Control to activate the Supercapacitor pack when the power demand varies rapidly, preserving the battery from degradation and harnessing the fast dynamics of the newly introduced component.
- The voltage of the Supercapacitor is assessed for precise utilization, ensuring that it is not employed when its voltage is below the set threshold. This approach guarantees that the SC is always available to deliver power.

In the event that the EM requires positive power, meaning that the vehicle is in traction, the RBC draws power from the supercapacitor if the power demand or the derivative of the power demand exceeds their respective thresholds.
If the power demand is negative (regenerative braking), the SC pack takes priority for recharging over the battery if the voltage is below the upper usage limit, to prevent its discharge, or if the derivative of power is higher than the threshold, to reduce stress on the battery.
To prevent the SC from discharging too quickly when used in traction, it delivers power equal to 80% of the required amount, leaving the remaining fraction to the battery. This approach effectively limits stress on the battery while conserving energy.
Finally, the power requested from the SC is increased when it is positive or decreased when it is negative, considering the presence of the bidirectional DCDC converter.
The Simulink block architecture is illustrated in Figure 15.

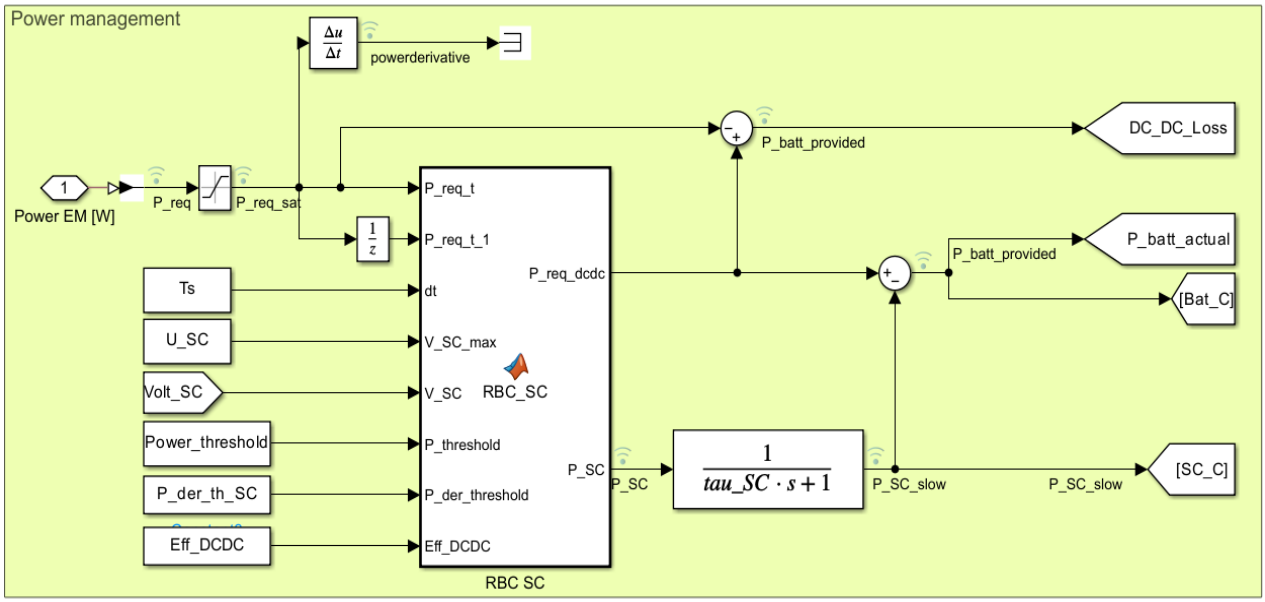

***Figure 15**: Simulink block architecture of RBC*

Supercapacitor voltage limits

Usually, the energy stored in a battery has a negligible effect on its voltage. Conversely, in a supercapacitor, the stored energy is directly proportional to the square of its voltage. Approximately 75% of the stored energy is consumed before the voltage reaches the usable range of 50%. Therefore, in practical design applications, the maximum usable energy for a capacitor is often calculated based on a voltage window of 50% of total V_{SC} [39]. In this study, it was decided to charge the supercapacitor through regenerative braking up to 90% of its maximum voltage. This allows space to store any extra energy in case the power exhibits a derivative higher than the set threshold, which could potentially cause more damage to the battery. The lower limit is set at 40% of the maximum voltage to maximize the utilization of stored energy.

Power threshold evaluation

To determine the Power Threshold value, P_{th}, first the evolution of the power request has been plotted (Figure 16), considering the mass of the vehicle M=13000 kg, over the Manhattan drive cycle.

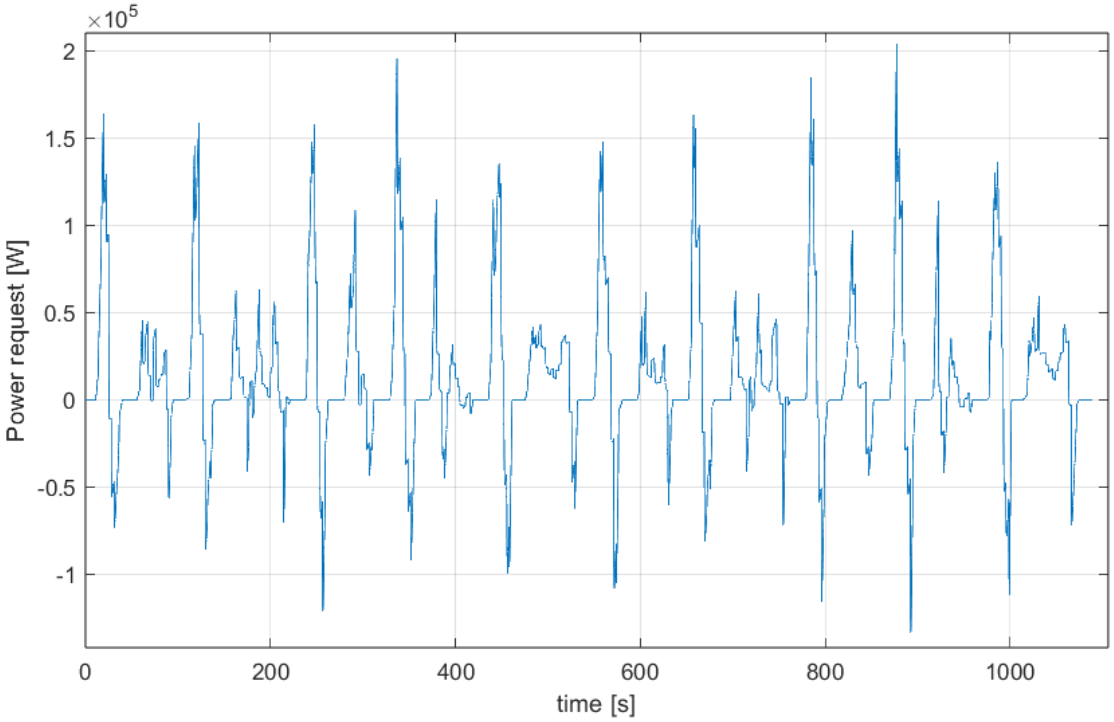

***Figure 16**: Power request for M=13000kg over the Manhattan drive cycle*

It can be observed that most of the peaks of power demand have values distributed between 60 and 160 kW. For this reason, a Design of Experiments (DOE) was conducted using values within this range. The Root Mean Square (RMS) value of the battery C-rate is evaluated for each P_{th} value, and are reported in Figure 17.

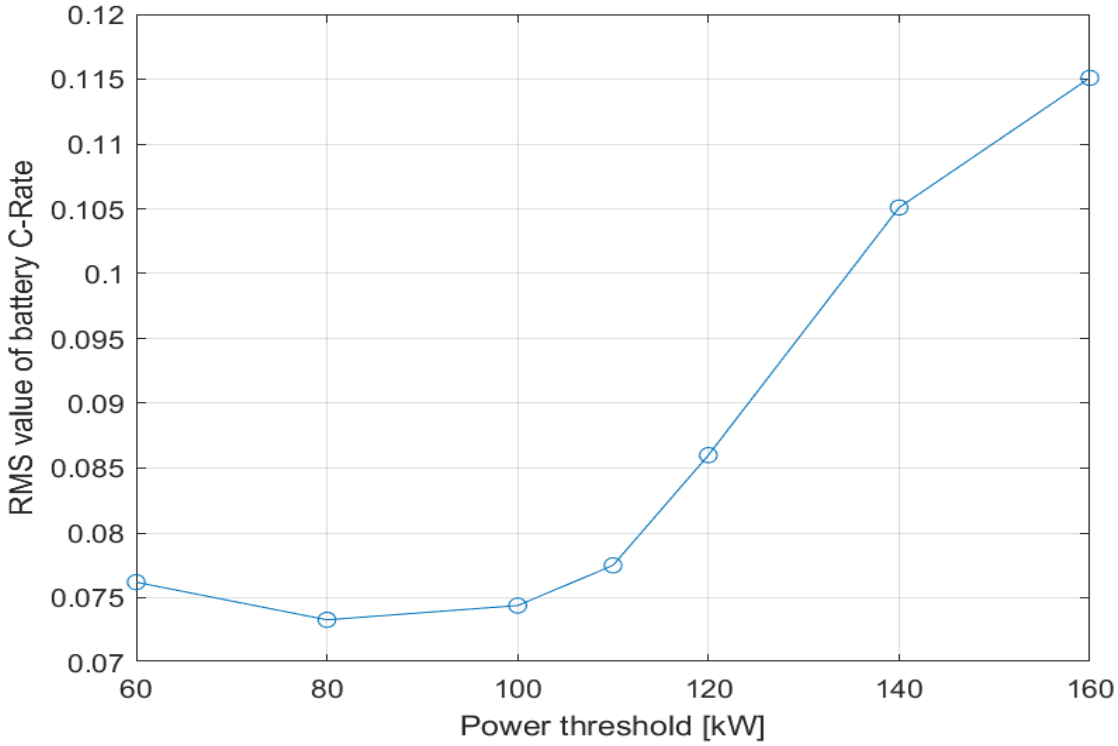

***Figure 17**: RMS of battery C-rate values changing Power threshold value*

For lower threshold values, lower battery C-rate values correspond, as the SC is used more frequently. However, it is essential that the voltage of the SC at the end of the simulation is at a level that allows it to be continuously used under these conditions. The voltage trends of the SC for various selected power thresholds are shown in Figure 18. Values of P_{th} = 60, 80, 100, 110 kW cannot be accepted, as they indicate that the SC discharges too quickly.

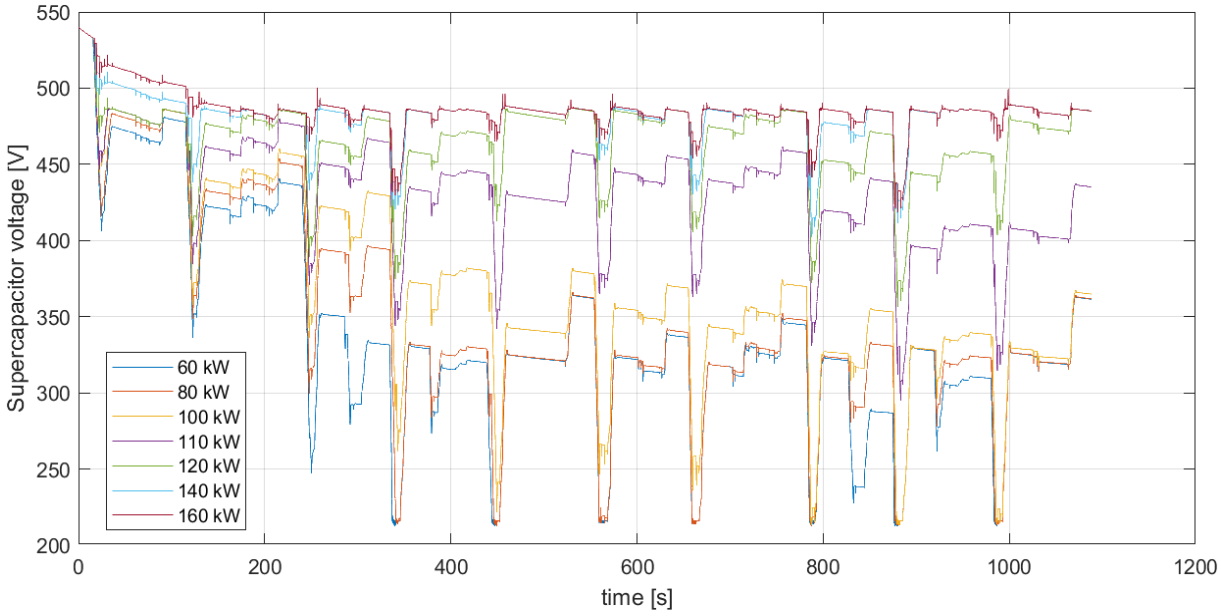

***Figure 18**: SC voltage during Manhattan drive cycle for different power threshold*

For these reasons, the value of P_{th} that minimizes stress on the battery while ensuring that the supercapacitor does not discharge is P_{th} =120 kW.

Power Derivative threshold evaluation

Similar analysis was conducted for calculating the power derivative threshold, P'_{th}. Figure 19 illustrates the evolution of the power derivative over the Manhattan drive cycle for a mass of m=13000kg.

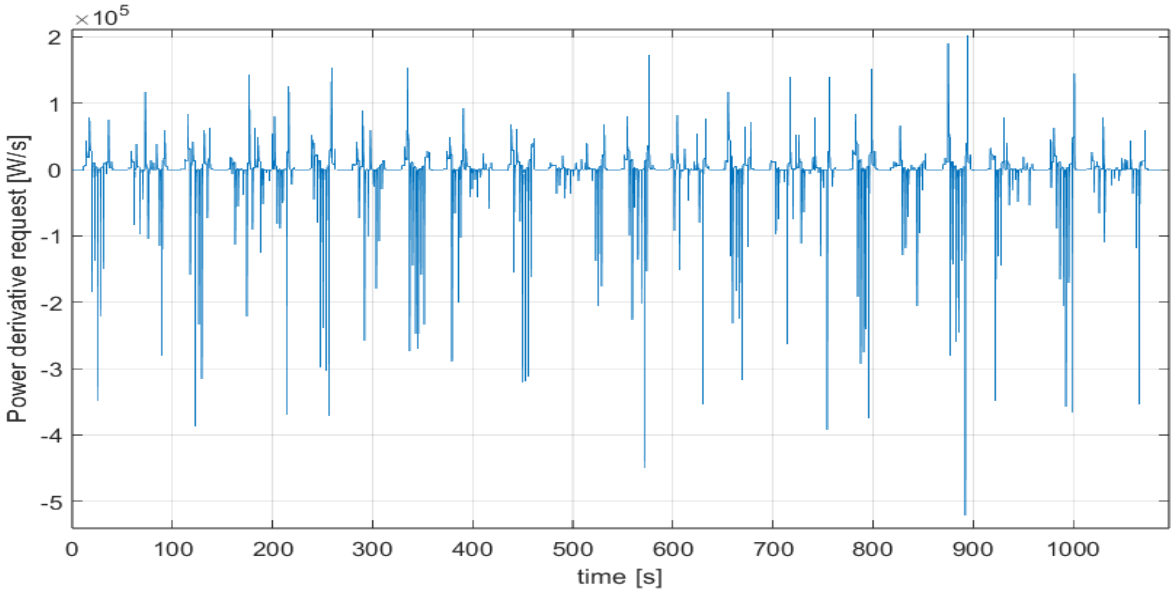

***Figure 19**: Power derivative request over Manhattan drive cycle for M=13000kg*

The figure emphasizes that the majority of peaks are in the order of magnitude of 10^5 W/s. Consequently, the DOE has been conducted with values of P'_{th} ranging from 10 kW/s to 100 kW/s.

As in the previous section, the RMS value of battery C-rate has been calculated for various P'_{th} values. (Figure 20)

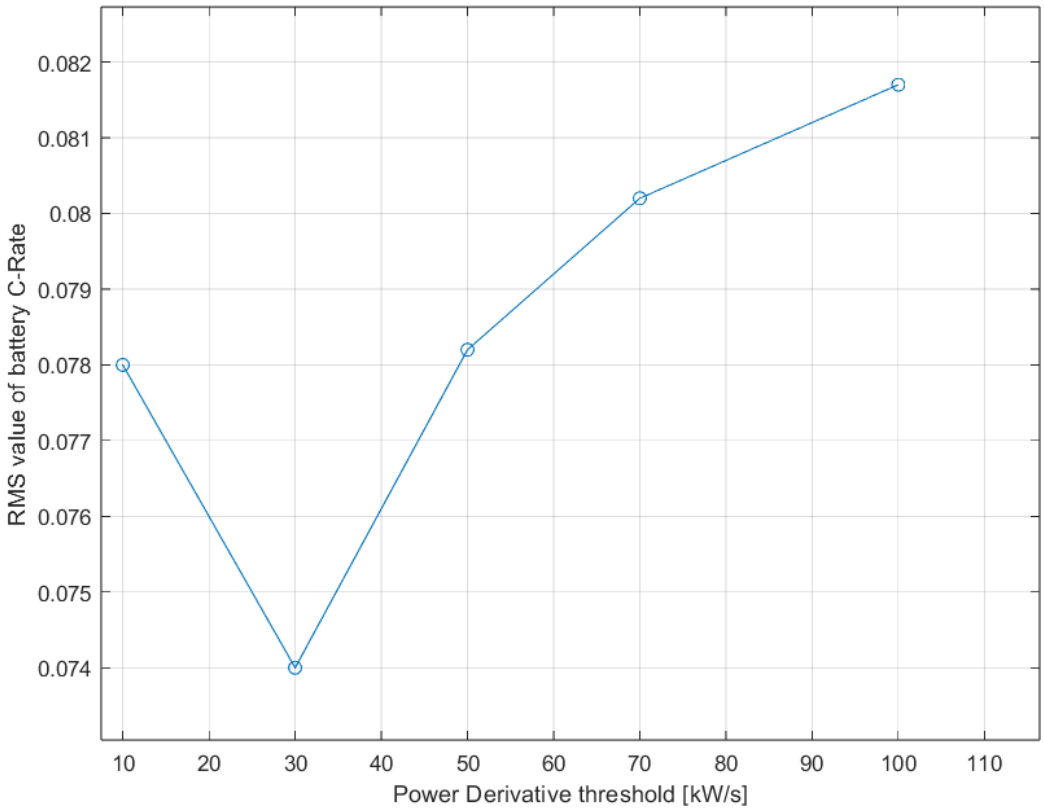

***Figure 20**: RMS of battery C-rate values changing Power derivative threshold value*

Once again, it is essential to assess the voltage of the SC at the end of the simulation to ensure charge-sustaining behavior. (Figure 21)

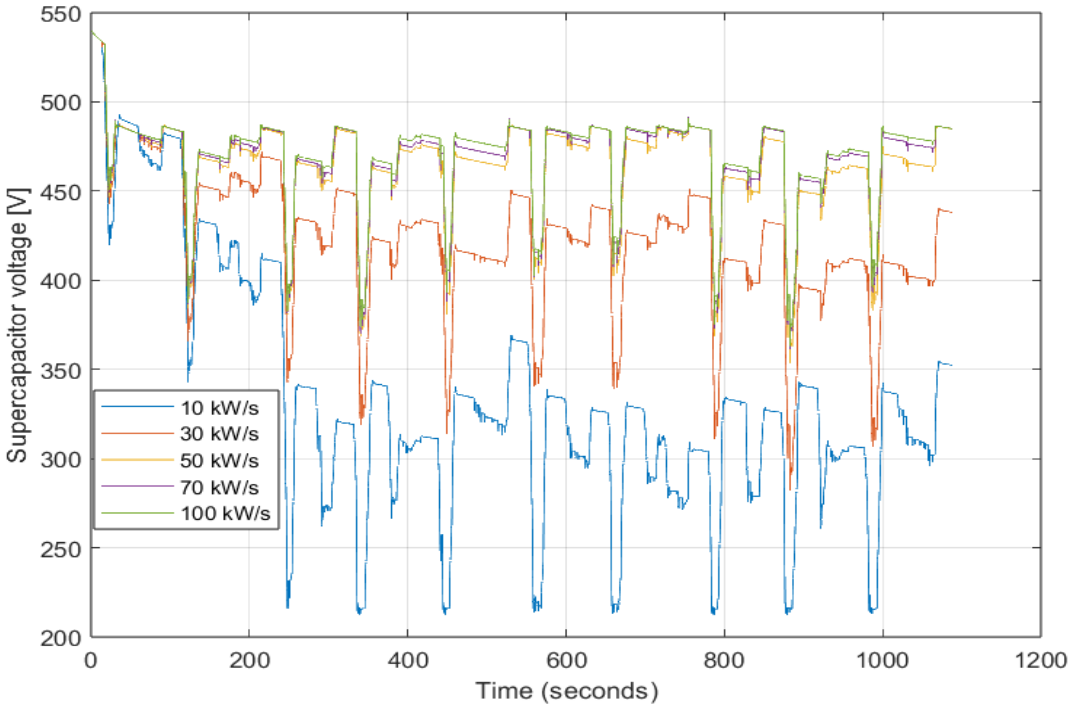

***Figure 21**: SC voltage during Manhattan drive cycle for different P'_{th}*

The optimal value for P'_{th}, which reduces stress on the battery while maintaining the required charge level on the SC, is found to be P'_{th} = 50000 W/s.

Adaptive Rule Based Control

The RBC has been developed by optimizing its parameters, namely the thresholds used, based on simulations conducted on a specific drive cycle, the Manhattan drive cycle. The previous RB control strategy has been improved to adapt to different drive cycles.

The new strategy, called Adaptive Rule-Based Control Strategy, revolves around the concept of adjusting the controller's power derivative threshold. This adjustment is made indirectly by considering the power demand of the drive cycle. The controller is made adaptive by introducing two counters that manage to describe the frequency with which the SC is called for use. Based on this information, the controller is able to vary the threshold to use the SC more efficiently. In Figure 22 the pseudo code of the A-RBC for computing the new threshold value.

```
SET counter1 = 0
SET counter2 = 0
FOR each time step
  INPUT powerRequest, voltageSC
  IF powerRequest is different from 0 THEN
     INCREMENT counter 1
  END IF
   IF SuperCapacitor is used THEN
      INCREMENT counter 2
   END IF
   IF voltageSC < 45% of maximum voltage THEN
      INCREMENT counter 2 by 10
   ENF IF
   COMPUTE ratio=counter2/counter1
   COMPUTE eps=10*ratio
   UPDATE powerDerivativeThreshold = powerDerivativeThreshold*eps
END FOR
```

***Figure 22**: A-RBC pseudocode*

When the ratio increases, indicating a more frequent use of the supercapacitor, the threshold value also increases, and conversely, when the ratio decreases. This approach allows for more frequent utilization of the SC in a drive cycle that would otherwise involve less frequent use according to the Rule-Based Control. By lowering

the threshold for power derivative, the adaptive strategy permits increased SC utilization in drive cycles where RBC suggests infrequent use, with benefits in reduced battery degradation. Conversely, in a drive cycle that demands excessive SC usage according to the RBC, the Power Derivative Threshold can be increased to avoid over-discharging the SC. In Figure 23 is presented the implementation of A-RBC in Simulink.

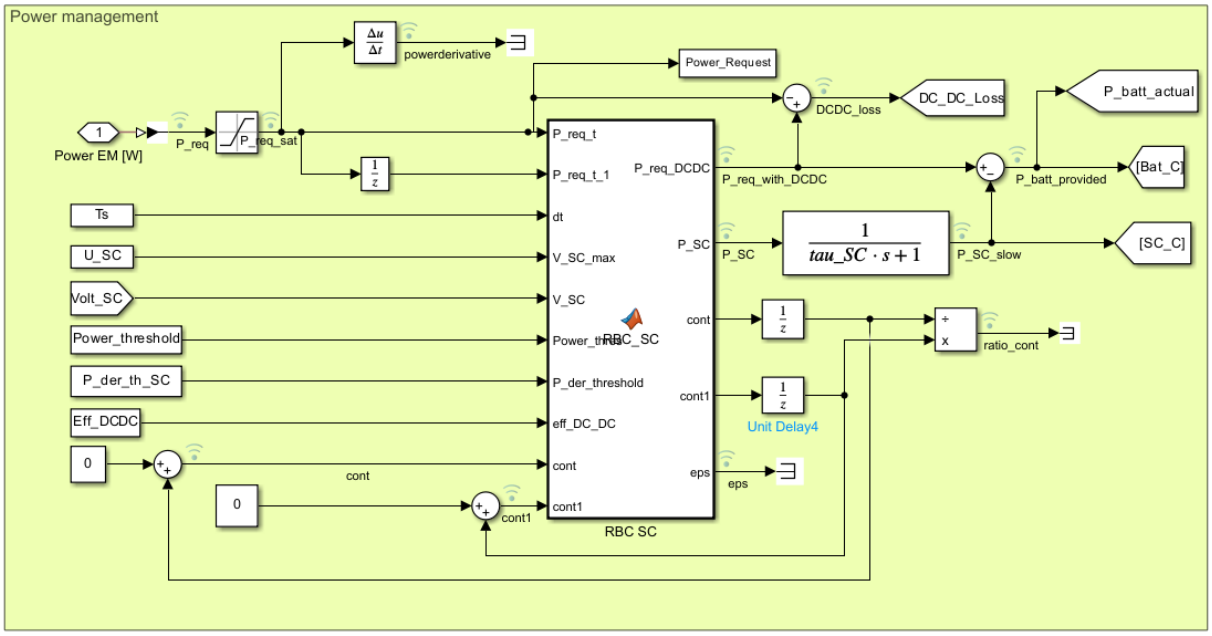

***Figure 23**: Simulink block architecture for A-RBC*

Fuzzy Logic Control

The third energy management strategy analyzed is based on fuzzy logic. The advantages obtained by using a Fuzzy Logic Controller are the ability to continuously control the power output from different sources and its convenience in design. It excels at modeling complex system behavior effortlessly through the use of expert knowledge-based rules. Indeed, it makes it very easy to use another input to adjust the power distribution, namely the vehicle's mass.

Structure

In this thesis, the Sugeno fuzzy inference system has been utilized and preferred over the Mamdani inference system. The two methods share similarities in various aspects: the initial two steps in the fuzzy inference process, involving the fuzzification of inputs and the application of the fuzzy operator, remain consistent between Mamdani and Sugeno. The primary distinction lies in the fact that Sugeno's output membership functions are either linear or constant.

Despite Mamdani being more intuitive and widespread, the choice fell on Sugeno because it is more compact and computationally efficient, and it works well with linear techniques, such as PID control.

Inputs

The Fuzzy Inference System has 4 inputs and provides as output the power delivered by the SC.

1. Supercapacitor's voltage (voltage_sc): this input has been split into three membership function: "LowVoltage," indicating a voltage lower than 215 V, which is 40% of the maximum voltage; "MediumVoltage," representing the usage range between 40% and 90%; and "HighVoltage," indicating a voltage exceeding 90%. (Figure 24)

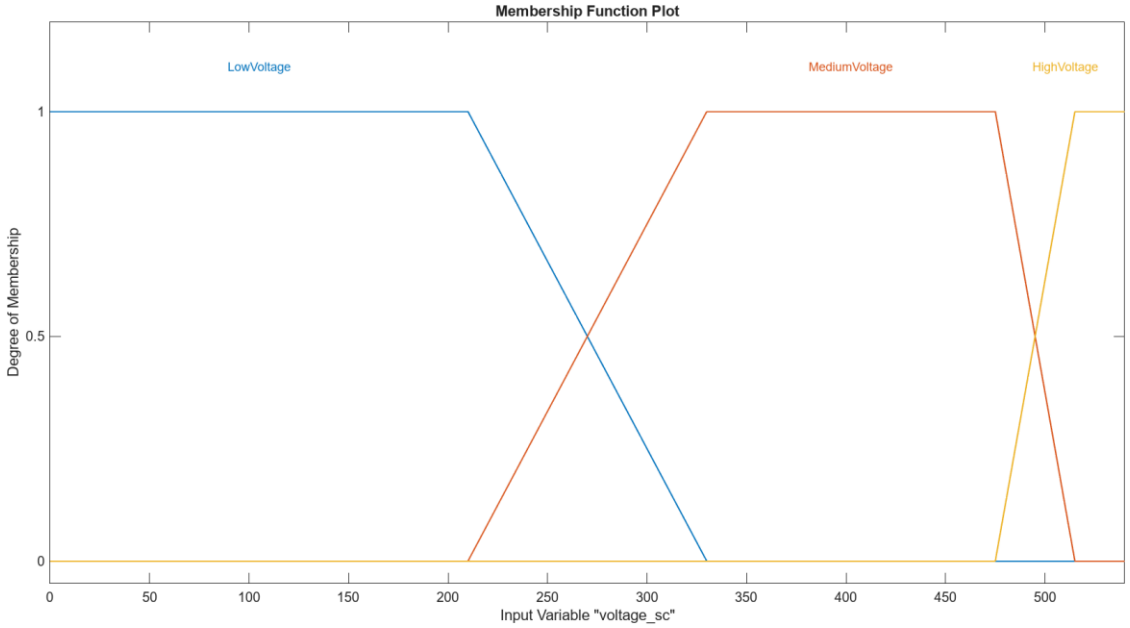

***Figure 24**:voltage_sc degrees of memebership*

2. Power request (Power_req): The power demand, on the other hand, has been divided into six membership functions, namely: "NegativePower", "VeryLowPower", "LowPower", "MediumPower", "HighPower", and "VeryHighPower". The use of different membership functions allows for a more precise control over the output. (Figure 25)

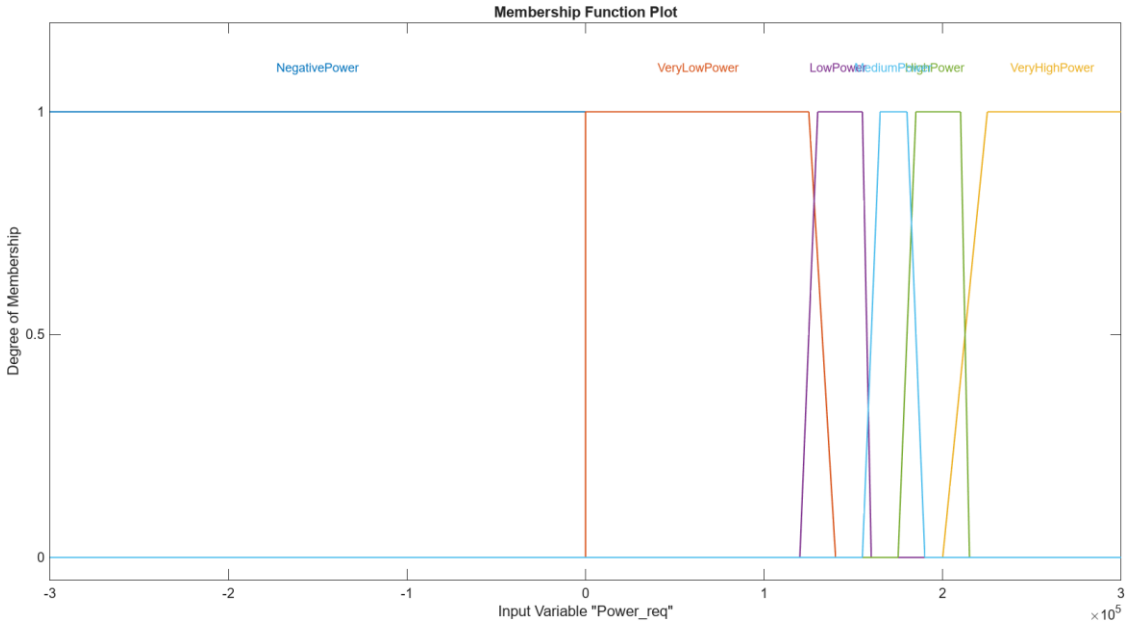

***Figure 25**: Power_req degrees of membership*

3. Power Derivative Request (Power_der): Three membership functions cover the entire range of power derivative: "Deceleration," representing power with a negative derivative less than -P'th; "LowDerivative," a derivative ranging between -P'th and +P'th; and finally, "Acceleration," indicating a power derivative greater than P'th. (Figure 26)

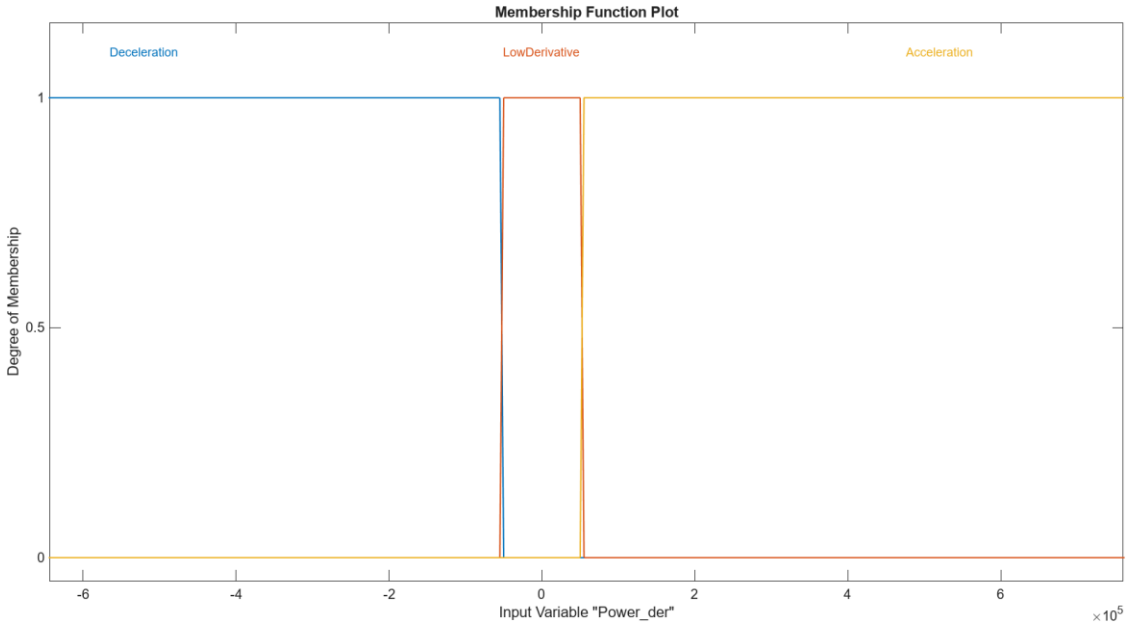

***Figure 26**: Power_der degrees of memebership*

4. Vehicle Mass (Mass): the mass range is divided into four membership functions, namely: LowMass, MediumMass, HighMass, VeryHighMass. (Figure 27)

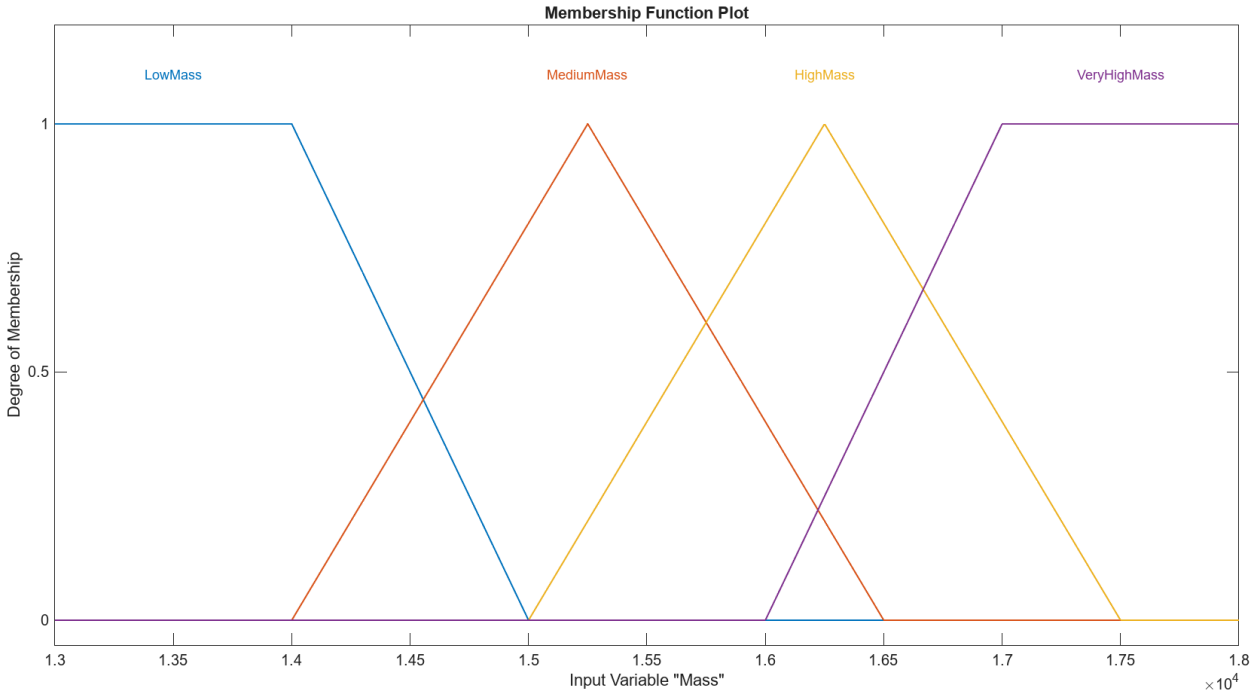

***Figure 27**: Mass degrees of membership*

Output

The only output of the fuzzy logic-based EMS is a value ranging from -1 to 1. This value is then multiplied by the absolute value of the power requested to generate the requested power value for the SC pack. As defuzzification method, the weighted average of all rule output has been chosen. In Figure 28 the rules designed for this FLC are presented.

	Rule	Weight	Name
1	If voltage_sc is not HighVoltage and Power_req is NegativePower then Power_SC is NegativePowerSC	1	rule1
2	If voltage_sc is not LowVoltage and Power_req is NegativePower and Power_der is not LowDerivative then Power_SC is NegativePowerSC	1	rule2
3	If voltage_sc is HighVoltage and Power_req is NegativePower then Power_SC is ZeroPowerSC	1	rule3
4	If voltage_sc is not LowVoltage and Power_req is not NegativePower and Power_der is not LowDerivative then Power_SC is PositivePowerSC	1	rule4
5	If voltage_sc is not LowVoltage and Power_req is LowPower and Mass is LowMass then Power_SC is PositivePowerSC	1	rule5
6	If voltage_sc is LowVoltage then Power_SC is ZeroPowerSC	1	rule6
7	If voltage_sc is not LowVoltage and Power_req is VeryLowPower and Power_der is LowDerivative then Power_SC is ZeroPowerSC	1	rule7
8	If voltage_sc is not LowVoltage and Power_req is MediumPower and Mass is MediumMass then Power_SC is PositivePowerSC	1	rule8
9	If voltage_sc is not LowVoltage and Power_req is VeryHighPower then Power_SC is PositivePowerSC	1	rule9
10	If voltage_sc is not LowVoltage and Power_req is MediumPower and Mass is LowMass then Power_SC is PositivePowerSC	1	rule10
11	If voltage_sc is not LowVoltage and Power_req is HighPower and Mass is not VeryHighMass then Power_SC is PositivePowerSC	1	rule11
12	If voltage_sc is not LowVoltage and Power_req is LowPower and Power_der is LowDerivative and Mass is not LowMass then Power_SC is ZeroPowerSC	1	rule12
13	If voltage_sc is not LowVoltage and Power_req is MediumPower and Power_der is LowDerivative and Mass is HighMass then Power_SC is ZeroPowerSC	1	rule13
14	If voltage_sc is not LowVoltage and Power_req is MediumPower and Power_der is LowDerivative and Mass is VeryHighMass then Power_SC is ZeroPowerSC	1	rule14
15	If voltage_sc is not LowVoltage and Power_req is HighPower and Power_der is LowDerivative and Mass is VeryHighMass then Power_SC is ZeroPowerSC	1	rule15

***Figure 28**: if-then rules for the FLC*

After calculating the power from the SC, the battery power is obtained by subtracting the power provided by the SC pack from the total required power, as shown in Figure 29. In this case as well, the presence of a DCDC converter is taken into account by introducing power losses in the SC.

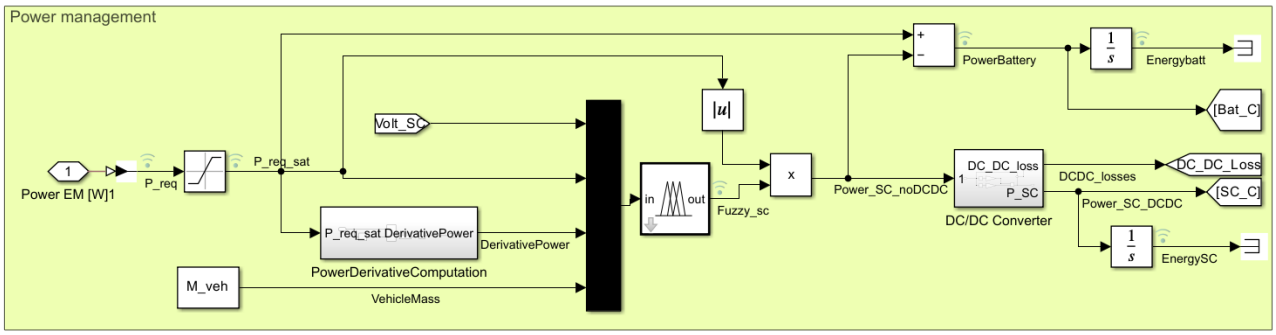

***Figure 29**: Simulink block architecture for FLC*

Simulation results

As previously mentioned, the primary aim in this initial phase of the thesis is to reduce the load experienced by the battery by introducing a SC, in order to extend its life. To validate the achievement of this objective and optimize the results, the different control strategies previously described will be compared:

- Battery Electric vehicle model
- Battery and SC HEV model with Rule-Based Control strategy
- Battery and SC HEV model with Adaptive Rule-Based Control strategy
- Battery and SC HEV model with Fuzzy Logic Controller strategy

The Battery Electric Vehicle model simulation results are used as baseline. The simulation is performed in the previously introduced Manhattan bus drive cycle with vehicle mass M=13000 kg.

Battery and Supercapacitor Hybrid Electric Vehicle with Rule Based Control

The results obtained by the simulation of the Hybrid model with RBC strategy are presented and compared with the ones of the BEV in Figure 30:

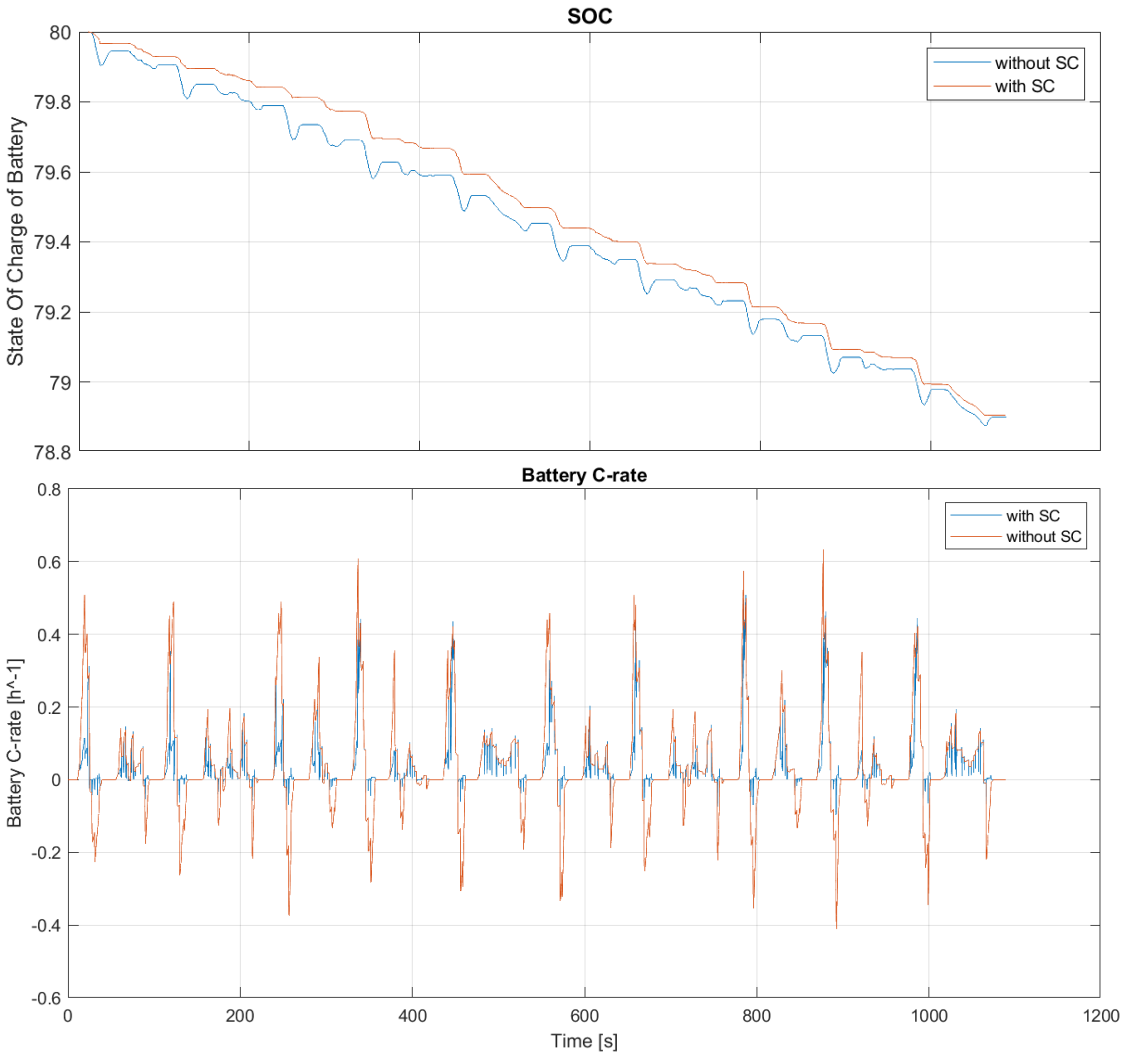

***Figure 30**: SOC and C-rate evolution for BEV and HEV with RBC*

The RMS relative difference of the C-rate is defined as:

$$RMS\% = \frac{RMS_y - RMS_x}{RMS_x} \times 100$$

where y and x represent the scenarios with and without the supercapacitor pack. The relative difference is calculated both for the State of Charge and for the RMS of C-rates experienced by the battery, and the results are summarized in Table 6:

	Unit	BEV	HEV	Relative difference
SOC reduction	- [%]	1.1	1.09	-0.9 %
RMS C-rate	[h^{-1}]	0.1316	0.086	-32.1 %

***Table 6**: SOC and Battery C-rate reduction with the introduction on SC*

As evident from the figure, the introduction of the SC pack does not bring significant benefits regarding the battery SOC (-0.9%). This is due to the fact that the energy introduced into the system by the SC pack is much smaller compared to that of the battery, owing to its low energy density characteristic. On the other hand, a notable reduction in C-rate is evident (-32.1%).

Comparison between Rule Base Control and Adaptive Rule Base Control strategies

The A-RBC was developed to ensure a robust EMS control strategy implemented by a rule-based controller, even in drive cycles different from the one used to optimize its parameters. For this reason, both the RBC and the A-RBC were tested in two new drive cycles to assess the adaptability of the latter. The two drive cycles used to test the A-RBC are described in Table 7:

	Parameter	Unit	Value
New York drive cycle	Total cycle time	s	600
	Maximum speed	m/s	12.3
	Maximum acceleration	m/s^2	2.22
	Covered distance	km	1.86
Singapore Route 91 drive cycle	Total cycle time	s	1600
	Maximum speed	m/s	11.3
	Maximum acceleration	m/s^2	1.7
	Covered distance	km	5.9

***Table 7**: New York and Singapore drive cycles parameters*

Firstly, the RBC and the A-RBC were compared on the Manhattan drive cycle. The evolution of the supercapacitor voltage is shown in Figure 31:

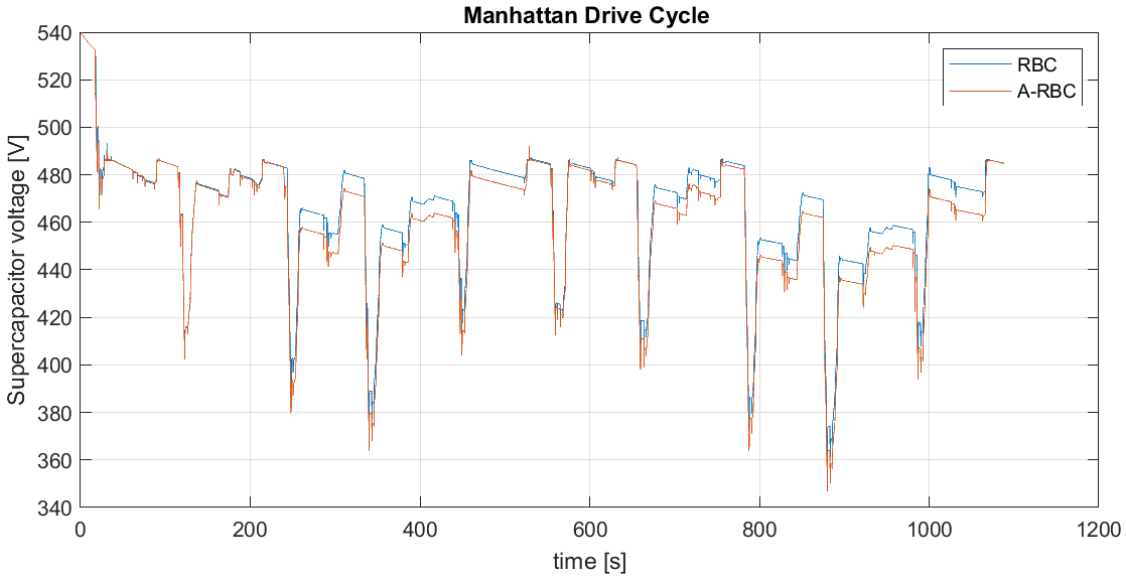

***Figure 31**: SC voltage evolution over Manhattan drive cycle for RBC and A-RBC*

It can be noted that there are no significant differences, as the RBC has already been optimized to operate with this specific drive cycle.

The two controllers are compared on a more aggressive drive cycle, the New York drive cycle. The trends of the supercapacitor voltage in the two cases are shown in Figure 32. In this situation, the A-RBC is capable of adapting to the high demand placed on the supercapacitor and modifying its parameters to preserve its charge. The energy is more effectively used by the SC: the adaptive control strategy prevents the

SC from using too much of its energy, thus enabling it to limit all local C-rate peaks, unlike the RBC.

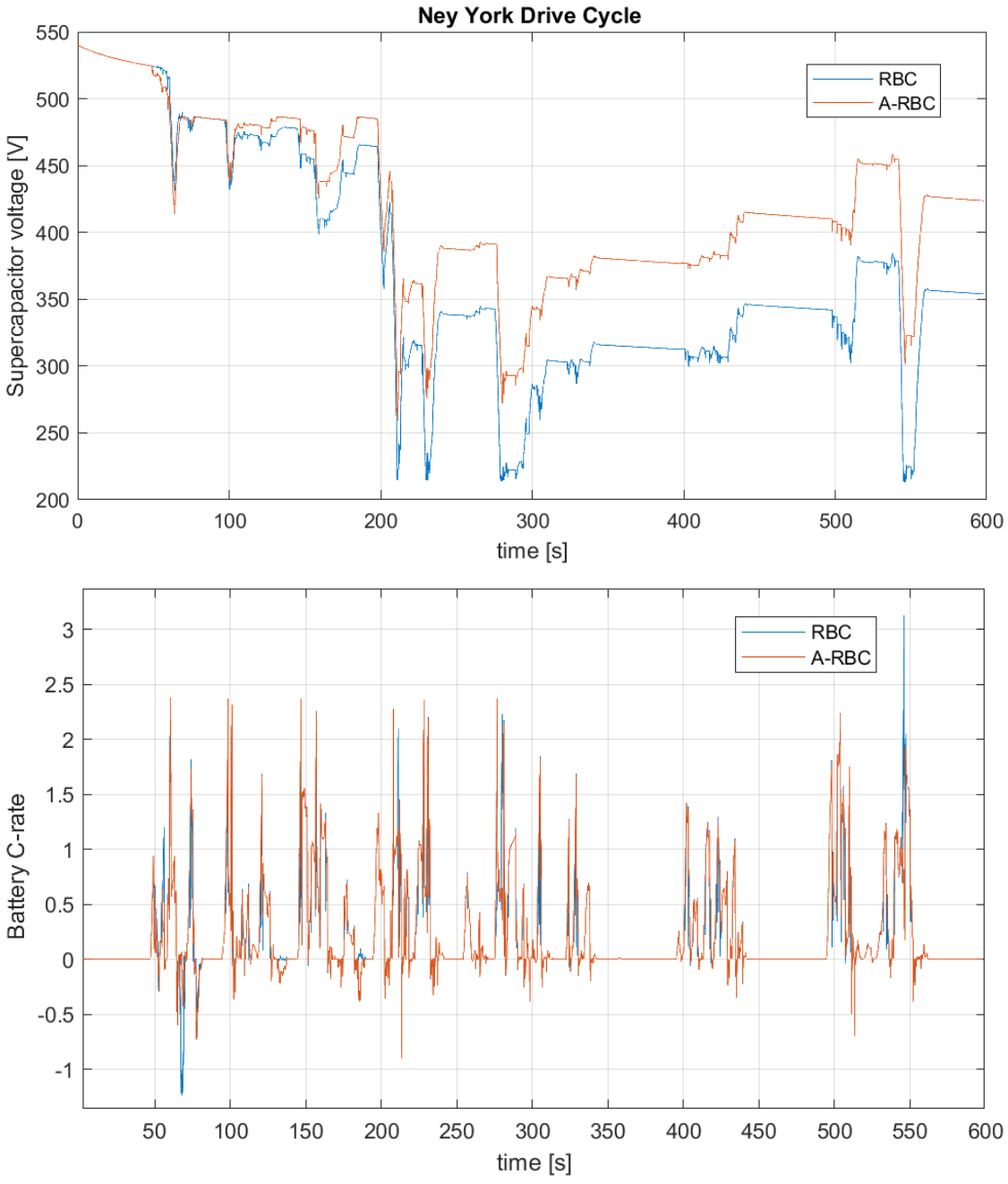

***Figure 32**: SC voltage and Battery C-rate evolution over New York drive cycle for RBC and A-RBC*

Finally, a less aggressive drive cycle, the Singapore one, is used. In this scenario, the initial rule-based controller is not able to effectively utilize the supercapacitor, while the adaptive one succeeds in doing so (Figure 33). This results in reduced stress on the battery, evidenced by a significant reduction in the RMS of the C-rate (Figure 34), while maintaining a high voltage across the supercapacitor.

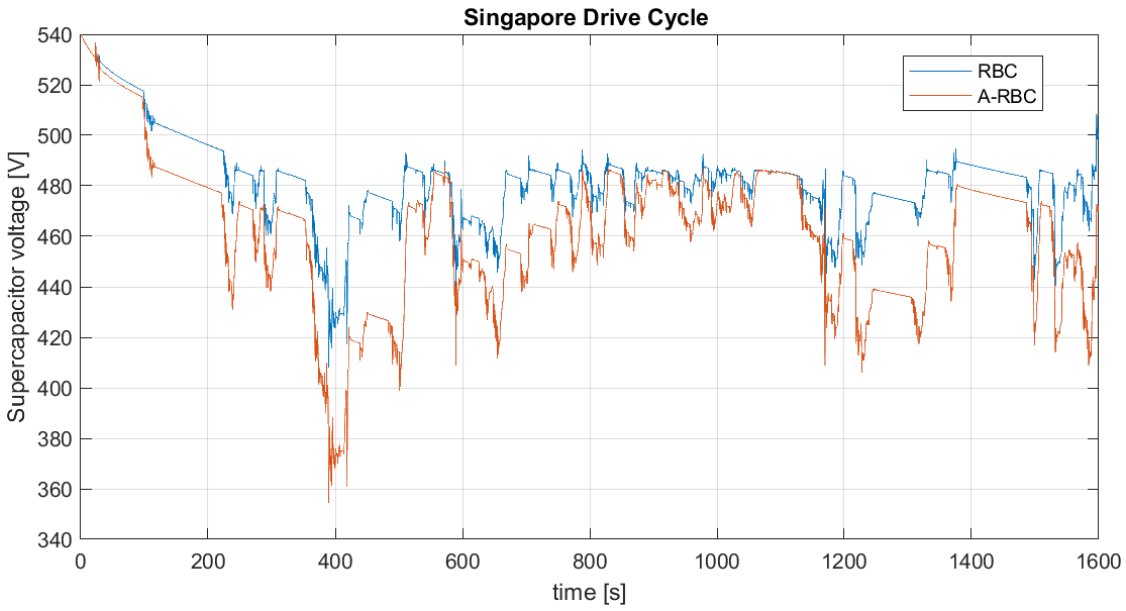

***Figure 33**: SC voltage evolution over Singapore drive cycle for RBC and A-RBC*

The RMS values of C-rate experienced by the battery in each scenario are reported in the graph below (Figure 34) and in Table 8 the relative differences between RMS values of C-rate are computed.

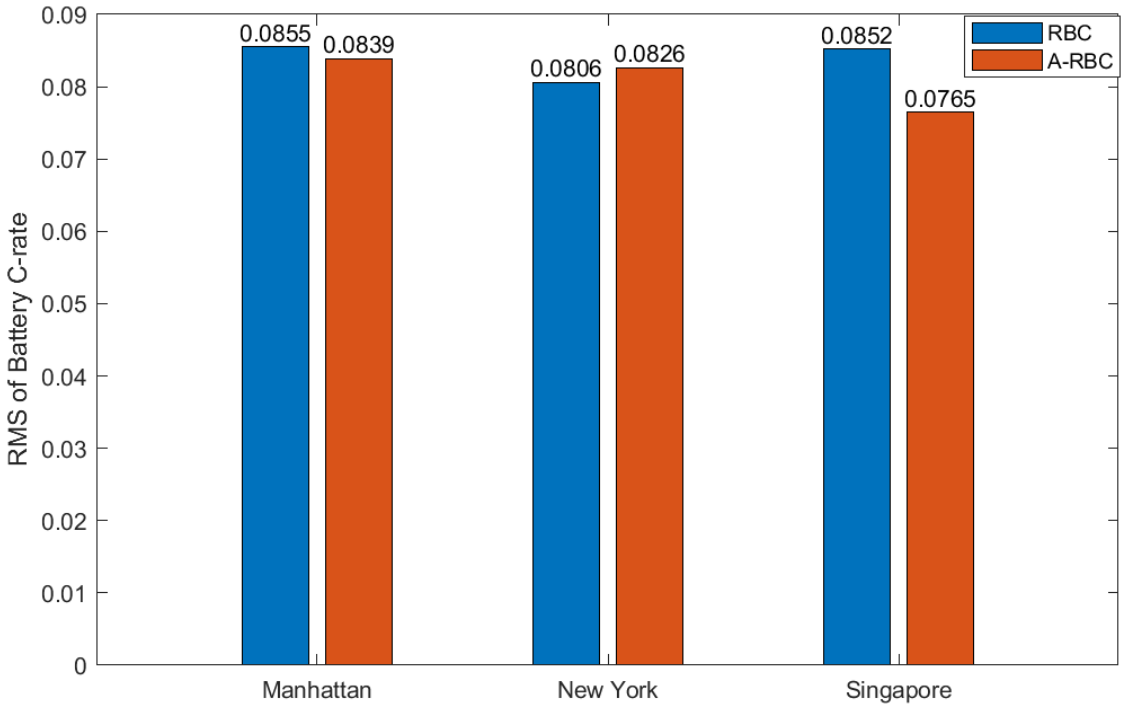

***Figure 34**: Bar chart reporting the C-rate RMS value over different drive cycles for RBC and A-RBC*

In the case of the Manhattan drive cycle, the difference is minimal, as previously mentioned since the RBC already performs very well in this scenario.

For the New York drive cycle, transitioning from RBC to A-RBC results in a slight increase in the C-rates experienced by the battery. This is due to the fact that the

supercapacitor is used less in the second case, preserving its charge to ensure availability when needed.

In the Singapore drive cycle, with A-RBC instead of RBC, there is a noticeable decrease in the C-rates experienced by the battery. The adaptive controller is capable of effectively utilizing the SC pack as much as possible assisting the battery pack.

	RBC	A-RBC	Relative difference
Manhattan	0.0855	0.0839	-1.87 %
New York	0.0806	0.0826	+2.48 %
Singapore	0.0852	0.0765	-10.2 %

***Table 8**: C-rate RMS values comparison for RBC and A-RBC over different drive cycles*

Comparison between Rule-Based Controller and Fuzzy Logic Controller for different mass values and drive cycle

The last energy management strategy developed is based on fuzzy logic. The idea is to create a controller that can easily adapt to variations in mass, a crucial requirement for a bus, which is constantly subject to passenger boarding and alighting. The fuzzy logic controller is well suited to this requirement, as it allows for the inclusion of the vehicle's mass as one of its input parameters.

The developed controller is simulated on the Manhattan drive cycle for three different mass values: 13000 kg, 14500 kg, and 15500 kg. The results were compared with those obtained from the Rule-Based control and are illustrated below, respectively in Figure 35, Figure 36, Figure 37.

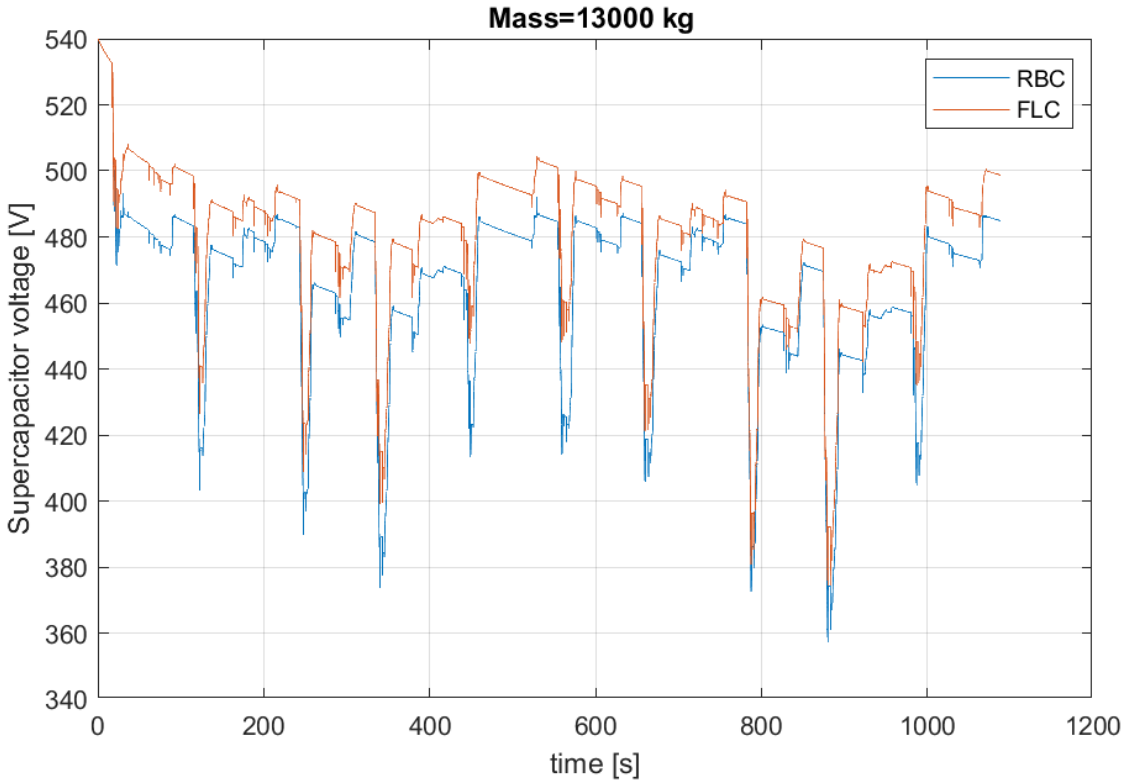

***Figure 35**: RBC and FLC SC voltage for M=13000 kg*

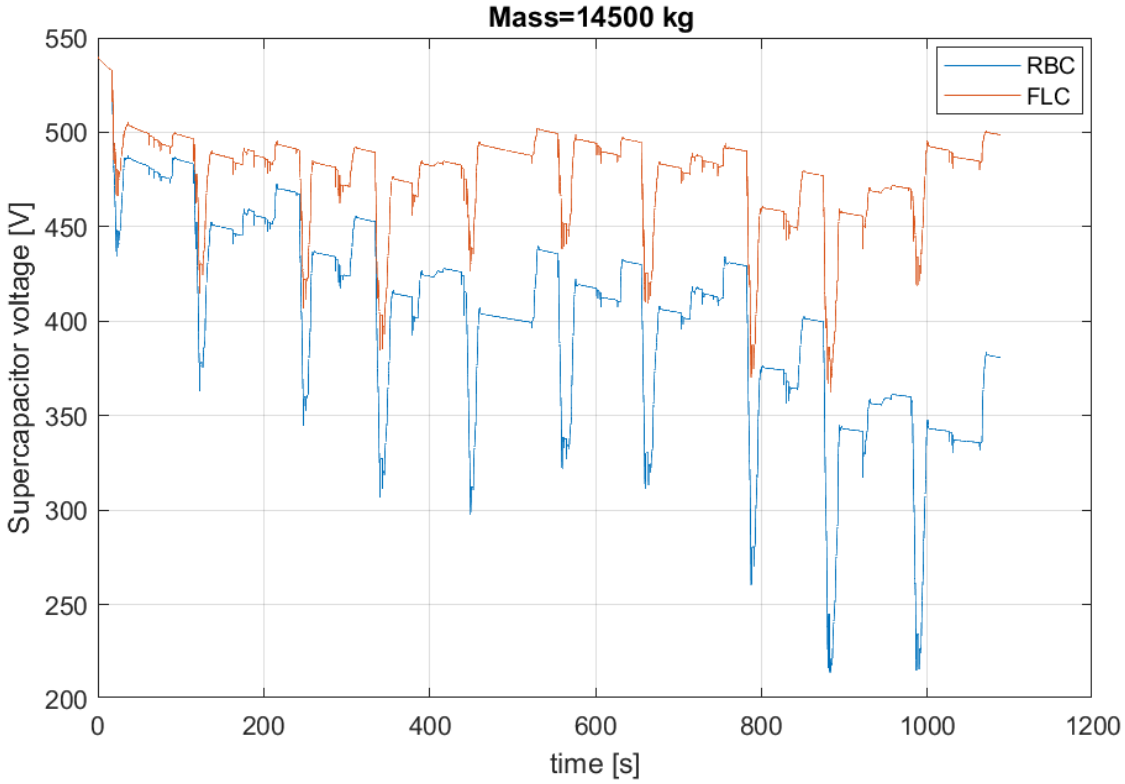

***Figure 36**: RBC and FLC SC voltage for M=14500 kg*

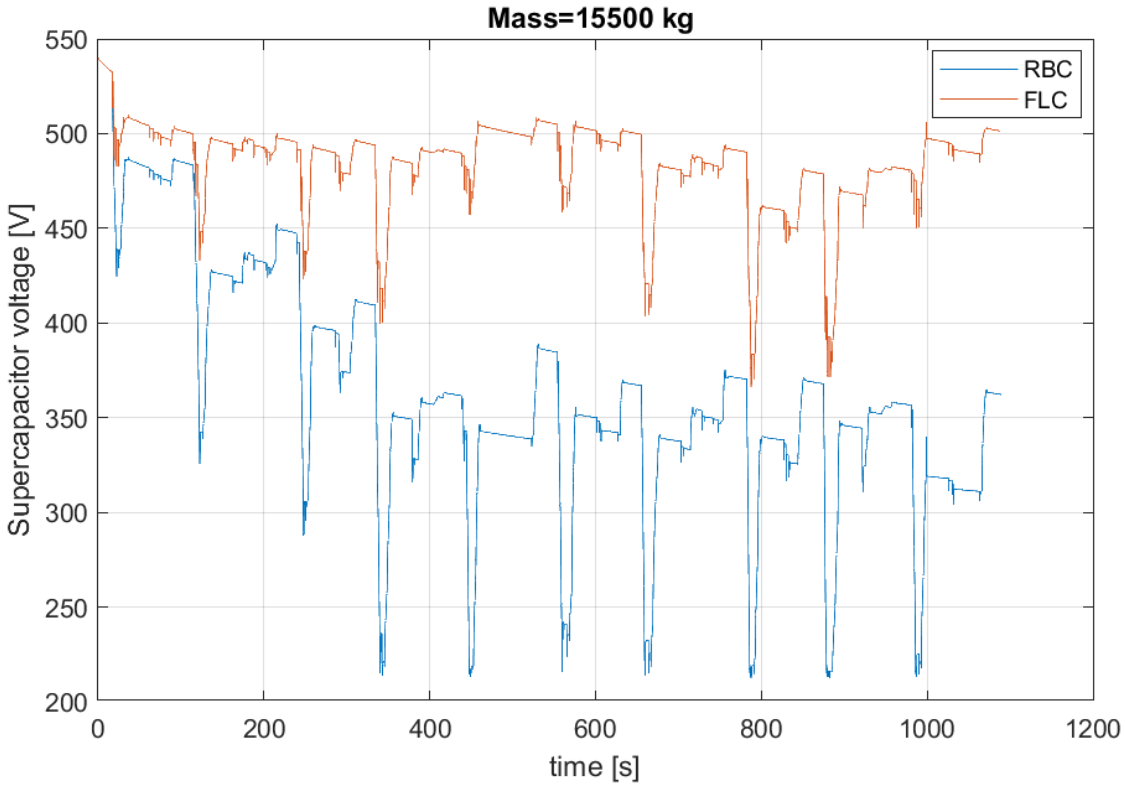

***Figure 37**: RBC and FLC SC voltage for M=15500 kg*

It is evident that the Rule-Based Controller is not able to use the supercapacitor pack correctly when the mass increases. In fact, the final voltage of the SC is very low in cases where m=14500 kg and m=15500 kg, indicating that it operates in a non-sustainable mode. On the other hand, the Fuzzy Logic Controller adapts perfectly to different masses, with the SC voltage showing an almost identical trend in various cases.

In Table 9, the RMS values of the battery C-rate are displayed. It is evident that the C-rates experienced during the simulation are higher in scenarios where EMS is implemented by the FLC. However, this is explained by the excessive utilization of the SC in the RBC logic, which eventually becomes depleted after a few minutes, no longer able to fulfill its role in assisting the battery.

Mass	RBC	FLC	Relative difference
13000 kg	0.086	0.090	+5.2%
14500 kg	0.084	0.097	+14.5 %
15500 kg	0.090	0.11	+15.3 %

***Table 9**: C-rate RMS value comparison between RBC and FLC for different mass values*

The fuzzy logic-based control strategy is also well-suited for adapting to different drive cycles. The model with the FLC was simulated over the New York drive cycle and compared with the adaptive rule-based controller. The SC voltage trends are shown in Figure 38.

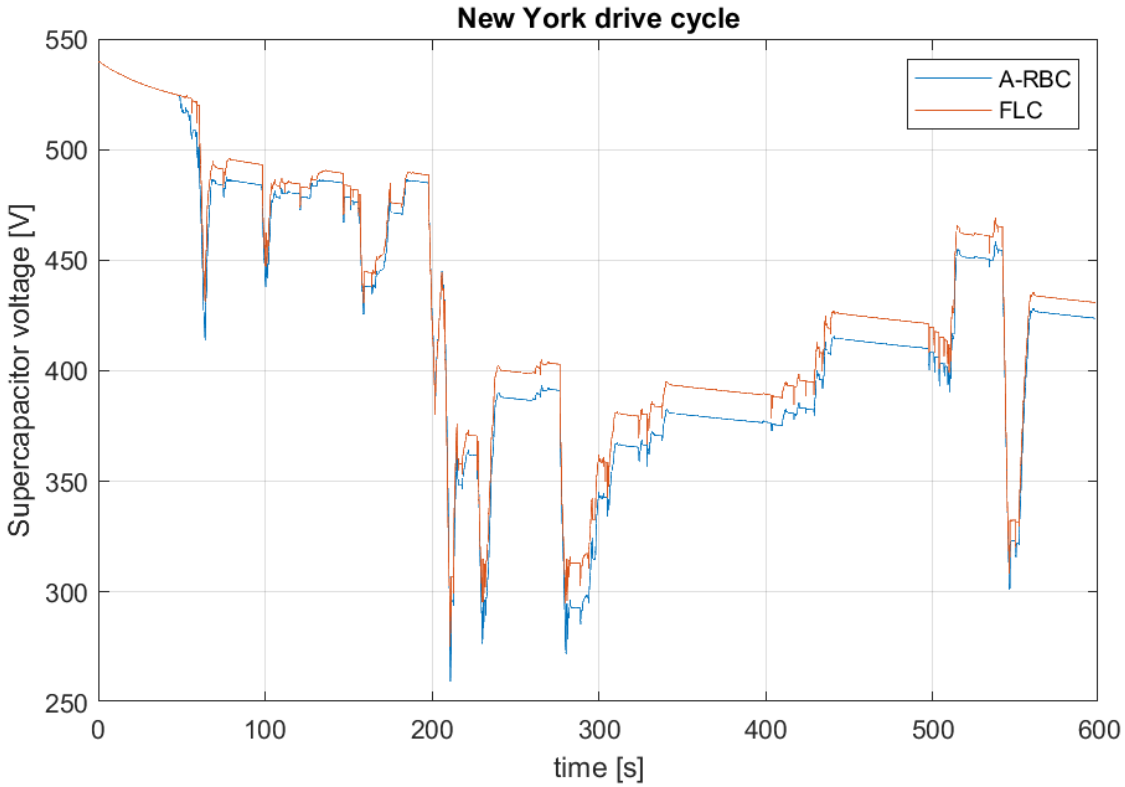

***Figure 38**: SC voltage evolution over New York drive cycle for FLC and A-RBC*

The two control techniques provide very similar results both in terms of their ability to manage the charge of the SC and regarding the battery C-rates experienced, as shown in Table 10 below.

	A-RBC	**FLC**	**Relative difference**
RMS C-rate	0.083	0.084	+2.1%

***Table 10**: C-rate RMS value comparison between RBC and FLC on New York drive cycle*

The Fuzzy Logic control strategy produces satisfactory results in terms of reducing the stress experienced by the battery as the vehicle mass and required payload vary.

II SECTION: Fuel Cell Hybrid Electric Vehicle

Fuel Cell Hybrid Electric Vehicle modelling

The second part of the thesis aims to model and test a Hybrid Energy Storage System based on a Fuel Cell Stack (FCS) and a battery pack. The goal is to reduce the size of the battery significantly, thereby decreasing the overall mass of the HESS. The charging rates of the new battery will thus be higher. For this reason, in order to limit them, a supercapacitor pack is later inserted in parallel.

Architecture

A Fuel Cell Hybrid Electric Vehicle incorporates multiple sources of energy, namely a Fuel Cell stack, a battery, and/or a supercapacitor pack. It is necessary to conduct an analysis of the various possible configurations and choose the most suitable one for the specific vehicle under consideration.

Parallel

In the first possible architecture, the power sources connected in parallel can directly supply power to the electric motor. In this case, schematized in Figure 39, the power flow is bidirectional for the battery and supercapacitor, as it allows regenerative braking through power absorption, while is unidirectional for the fuel cell stack.

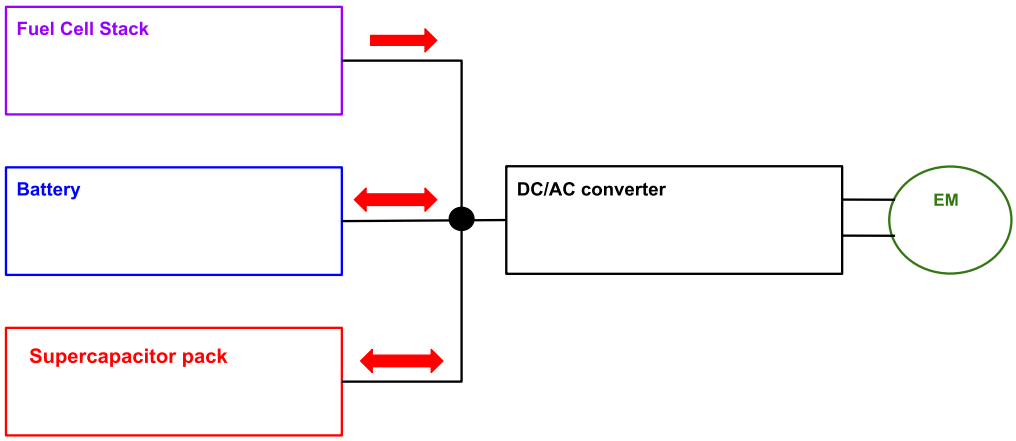

***Figure 39**: parallel architecture for a FCHEV*

The main disadvantage of this configuration is the complexity of the necessary control techniques. An example of this is the work of Fu et al .[31], where a two-layer control is implemented. The upper layer regulates the power required for the SC, while the lower layer manages the power split between the battery and the Fuel cell stack.

Series

In the series architecture, Figure 40, on the other hand, the Fuel cell stack does not directly supply power to the load but continuously charges the battery. The supercapacitor is still inserted in parallel with the battery to provide peak power and absorb braking energy with a high-power rate.

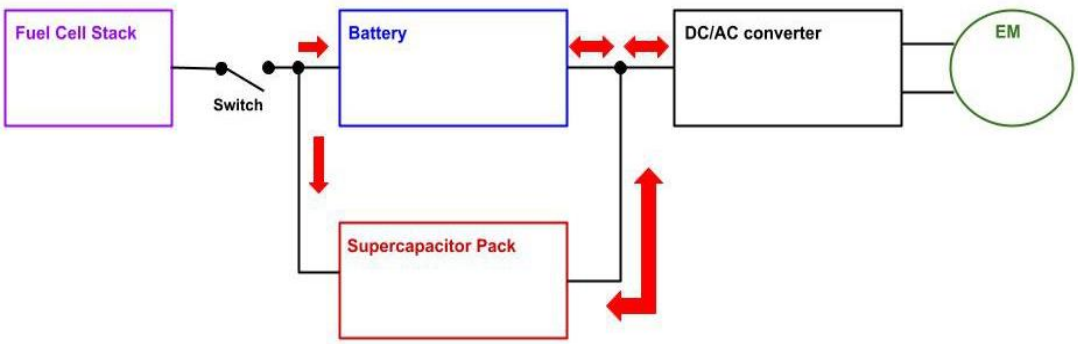

***Figure 40**: Series architecture implemented in this thesis*

The key benefit of this configuration is maintaining continuous operation of the Fuel Cell Stack by charging the battery. This helps avoid fluctuations in the power demand on the FCS, thereby addressing its primary limitation, which is its limited dynamic response.

In this thesis, the series architecture has been chosen due to its lower control complexity and because it is the most widely used in the literature.

Power source modeling

Once the utilized architecture has been defined, it is necessary to describe and model the power sources in place, namely the Fuel Cell Stack, the Battery Pack, and the Supercapacitor pack (Figure 41). Since the latter has already been described in the previous chapter and appears unchanged in this implementation, its description has been omitted.

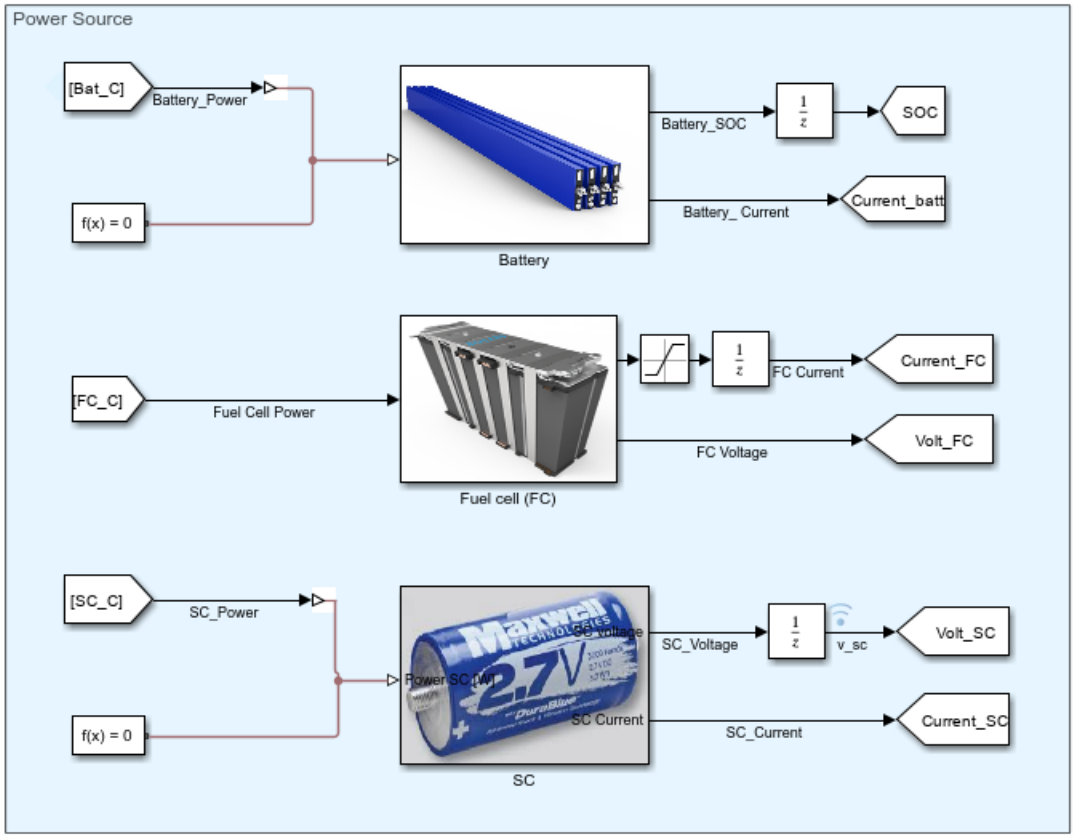

***Figure 41**: Power Source block scheme in Simulink*

Fuel Cell

The selected Fuel Cell Stack is the VL-40 model produced by Horizon Fuel Cell Technologies. The choice was made for this model as the VL series of FCS is currently powering trucks and buses in China [40]. The parameters of the FCS are described in Table 11.

Parameter	Unit	Value
Type of cell	-	PEM
Number of cells	-	220
System Rated Power	kW	40
Voltage Output	V	145
Current Output	A	400
Ambient temperature	°C	-30 - 45
Working temperature	°C	70 - 90
System Dimension	mm	890 x 600 x 520
Total FC System Weight	kg	145

***Table 11**: VL-40 FC system parameters*

The Simulink model of the FCS is based on two lookup tables that utilize two maps, namely a current efficiency map and a current voltage map, for a hydrogenic power module fuel cell appropriately scaled for the specific application under consideration (Figure 42). Despite the fact that the type of fuel cell does not match the actual chosen component, i.e., a PEM fuel cell, it can be asserted that the exhibited behavior

does not differ significantly. To assert this, the trends of the maps used were compared with those provided by Horizon for FCS of the same type but smaller in size, along with results obtained from literature for PEM fuel cells [41].

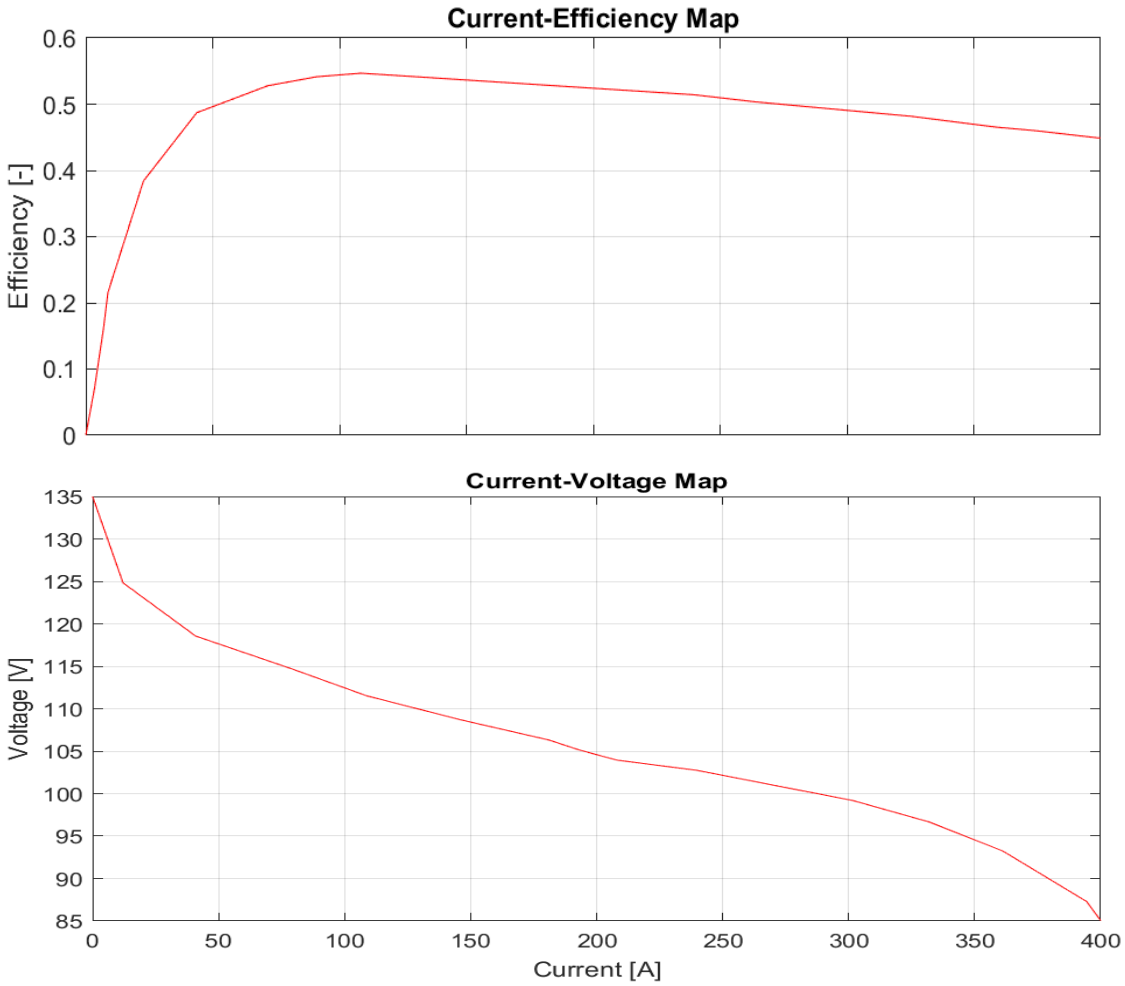

***Figure 42**: Current-Efficiency and Current-Voltage maps scaled*

The current-voltage map is used within the Simulink model of the FCS, as depicted in Figure 43. Starting from the received power commands as input, it outputs the voltage and current of the component.

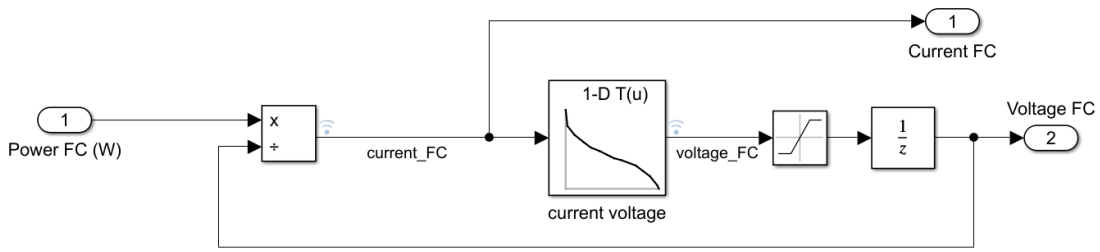

***Figure 43**: Fuel Cell Stack block scheme in Simulink*

To choose the appropriate size for the fuel cell stack, an analysis of the required energy was conducted. First, the total energy required by the Manhattan drive cycle was calculated (Figure 44).

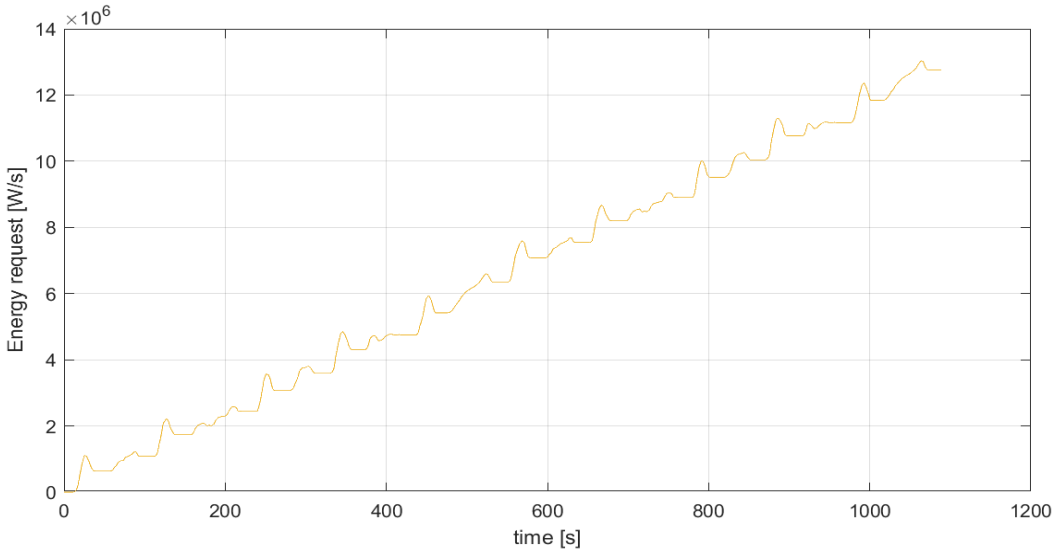

***Figure 44**: Energy request for Manhattan drive cycle*

Subsequently, the average power required P_{avg} was computed by simply dividing the total energy required in the cycle, that is 1.27e7 W/s, by its duration, 1090 s. Since the goal is to achieve charge-sustaining operation for the battery, a fuel cell stack was chosen with an output power at maximum efficiency close to the average power required by the drive cycle. The calculated average power P_{avg} is 11.7 kW, and for this reason, the Horizon VL-40 fuel cell stack with an output power at maximum efficiency $P_{\eta MAX}$=12.1 kW, very close to P_{avg}, has been chosen. The control mechanism for power will be described in more detail in the next section.

Battery downsizing

The use of the FCS as the primary energy source allows for a significant reduction in the size of the battery, which serves now as a power buffer. However, to maintain a degree of consistency in sizing the new battery, cells of the same type as those found in the actual battery of BYD K9 buses and previously described were chosen for the undersized battery pack. The cells used in the new downsized battery are still of the prismatic type, with the same voltage but reduced capacity. The characteristics are summarized in Table 12:

Parameter	Unit	Value
Chemistry	-	Lithium-Iron Phosphate
Type of cell	-	Prismatic
Rated capacity	Ah	100
Rated voltage	V	3.2
Weight	kg	1.95
Size	mm	121 x 160 x 49
Working temperature	°C	-20 - 60

***Table 12**: BYD C49 battery cell features*

The voltage of the entire battery pack remains unchanged, so the same number of cells in series is used, which is 169. As for the total capacity, it is reduced to one-sixth of the initial value, envisioning only one row composed of the new cells in parallel, resulting in a capacity of exactly 100 Ah.

The mass of the new battery is calculated by multiplying the weight of a single cell by the number of cells in series and in parallel. The obtained value is 330 kg. This downsizing process allows for a significant reduction in the battery mass while still maintaining a battery large enough to provide the required power without degrading too quickly.

Control techniques

In this section, power control strategies for the fuel cell stack will be analyzed to ensure charge-sustaining operation of the battery. In charge sustaining condition the initial battery State of Charge is almost equal to the final one. In this scenario, the battery is not recharged through a connection to the electric grid but rather by the Fuel Cell and absorbing excess energy through regenerative braking. This approach does not require long stops for electric charging but only refueling the hydrogen tank.

Rule Based Control

The first strategy involves regulating the power continuously sent from the fuel cell to the battery using a set of simple rules and includes two usage modes for the FCS.

- at maximum efficiency: when the SOC of the battery is within the range between the lower and upper limits (between 75% and 85%), the Fuel Cell provides power by operating at the point of maximum efficiency to reduce hydrogen consumption.
- at maximum power: when the SOC of the battery drops below the predefined limit (SOC < 75%), to ensure charge-sustaining operation, the Fuel Cell operates at maximum power, immediately increasing the battery charge level.

Both working points are shown in Figure 45.

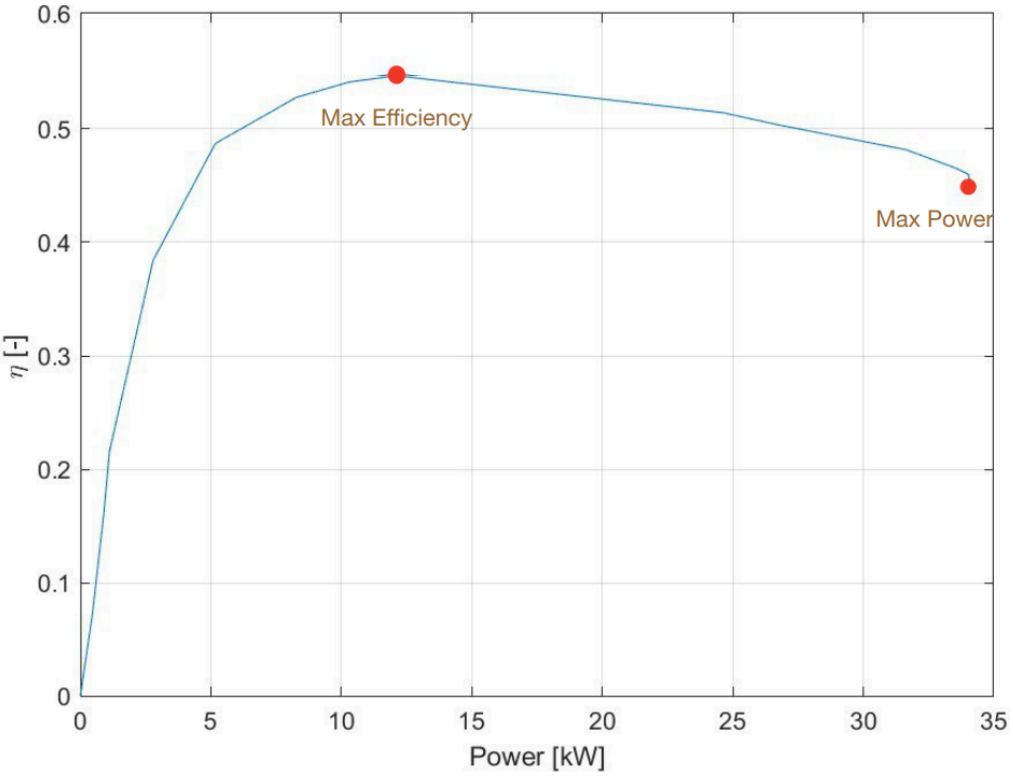

***Figure 45**: Operating points of the FCS with Rule Based Controller*

The SOC is kept in the range between 75 and 85% of the maximum one by the Rule Based Controller. When the battery SOC is at a level above 85%, the incoming power produced by the FCS at maximum efficiency is blocked by opening a switch. Due to the poor dynamic response of the fuel cell, it is preferable to lose the power delivered in the moments in which the battery is more charged than the upper limit rather than bringing the output power of the FC to 0, as this avoids the power transient for the FC.

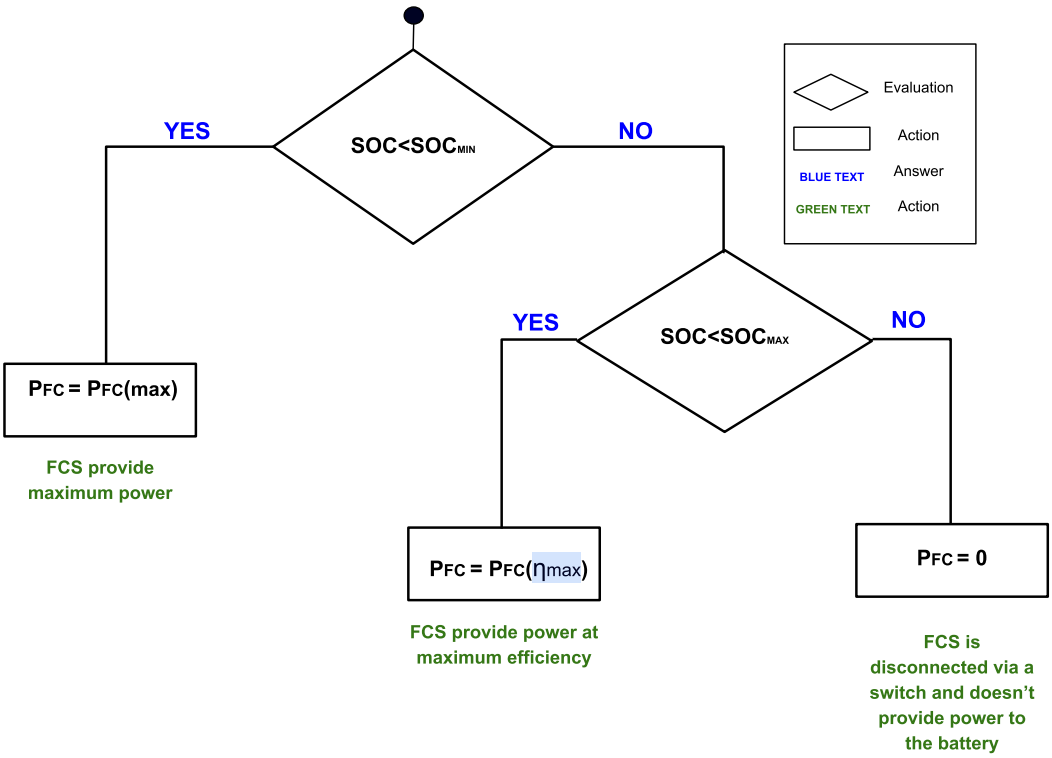

***Figure 46**: RBC flowchart*

To implement the RBC in Simulink, a MATLAB function block is used. The flowchart representing the RBC is shown in Figure 46.

Fuzzy Logic Control

In the control strategy just described, the Fuel Cell Stack operates only at two points, either at maximum power or at maximum efficiency. This allows the system to function in a charge-sustaining manner. However, due to the slow dynamics of the FC, a problem arises during moments when its operating point shifts, meaning where the power output is not continuous. If the power output from the FCS needs to change rapidly or significantly, performance problems in the system could occur like delays in the response. To address this issue, a Fuzzy Logic-based control strategy, that enable a smooth transition between different operating point in response to variations in power demand, is implemented. The operating range of the FC with the FLC is shown in Figure 47.

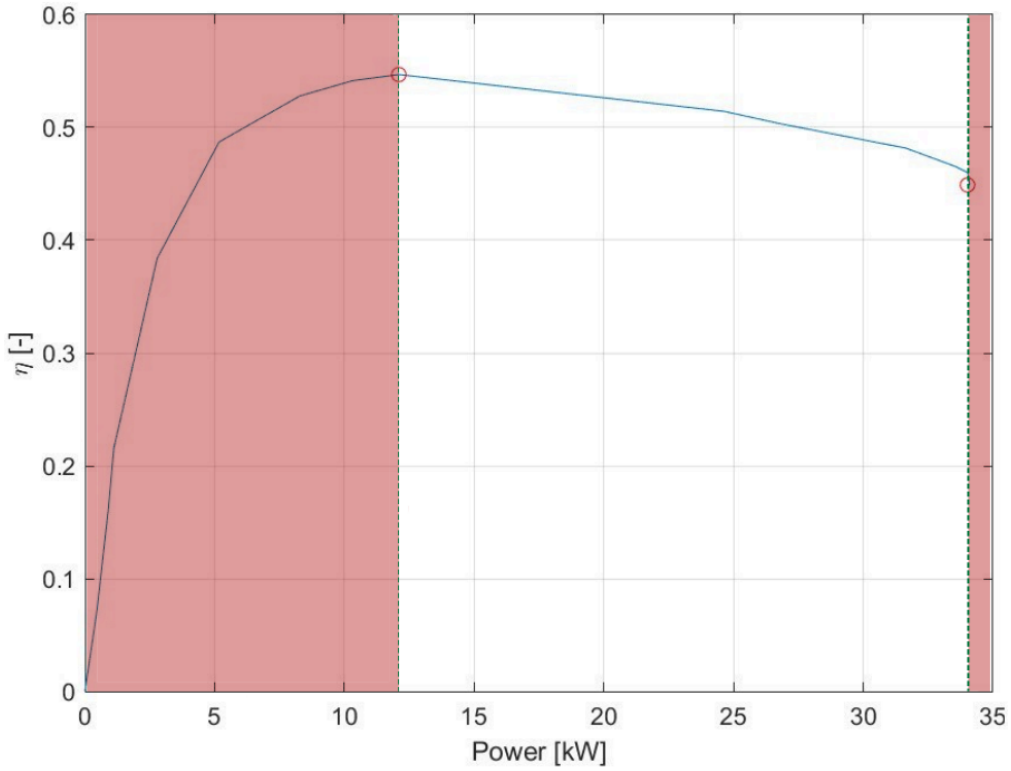

***Figure 47**: Operating range of FCS with Fuzzy Logic Controller*

The FLC operates by generating a command representing the output current value of the FC. The output of the Fuzzy Inference System block ranges from 0 to 1, where 0 represents the current at the maximum power operating point, while 1 represents the current at the maximum efficiency operating point. The current value is calculated using two gains that are summed as shown in Figure 48. For example, if one is close to the lower limit value of SoC, the output of the FIS will be a value close to 0, for instance, 0.2. This represents the fraction to be multiplied by the current at maximum efficiency, while 1-0.2=0.8 represents the fraction multiplied by the current at maximum power. In this way, the resulting current will be close to the maximum, corresponding to maximum power. As evident, the current range in which the FC is operating lies between the two points of maximum efficiency and power**Figure 48**.

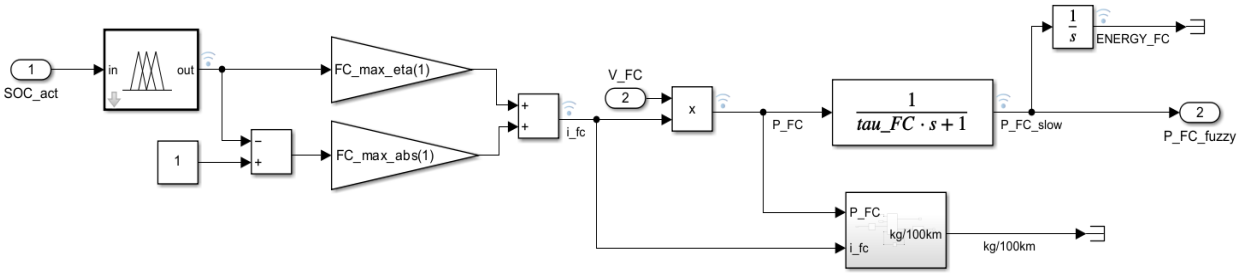

***Figure 48**: FLC block scheme in Simulink*

The fuel consumption by the FCS is then calculated based on the efficiency at each moment and is indicated in kilograms of hydrogen consumed per 100 kilometers traveled. The Fuzzy Inference System used is simpler than the one governing the SC

described in the previous chapter, as it has only one input, the battery SOC, whose membership functions are shown in the figure. For the same reasons mentioned earlier, the Sugeno type has been chosen over Mamdani one.

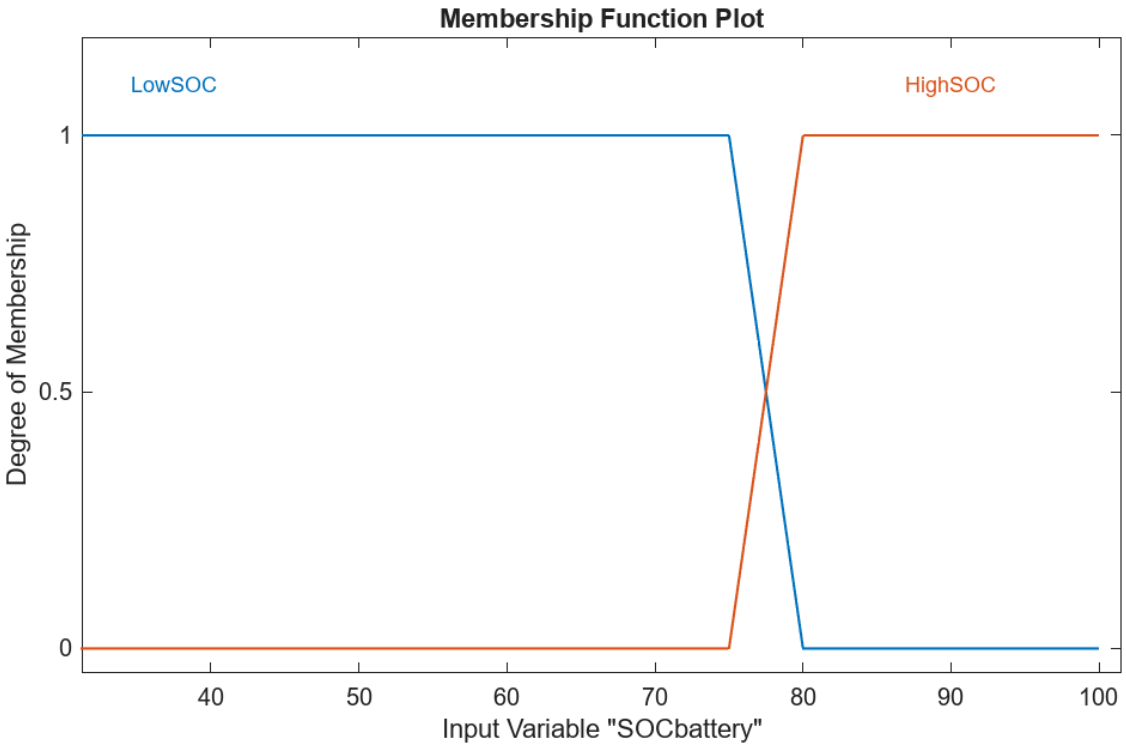

***Figure 49**: battery SOC degrees of membership*

"LowSOC" and "HighSOC" are the membership function for the input, with the first one reaching the SoC value of 75% before descending, while the second one starts rising at the same point (Figure 49). The only output is "PowerFuelCell," which can take two values, "MAX POWER" or "MAX EFF", corresponding to the output values of 0 and 1, respectively. The rule set consists of just two rules, namely:

- If SOCbattery is HighSOC then PowerFuelCell is MAX EFF
- If SOCbattery is LowSOC then PowerFuelCell is MAX POWER

Simulation results

Comparison between Rule Based Controller and Fuzzy Logic Controller

To compare the implemented strategies, the parameters taken into consideration are the battery SOC, which to operate in charge-sustaining mode must be within the range of 75 to 85%, and the fuel consumption.

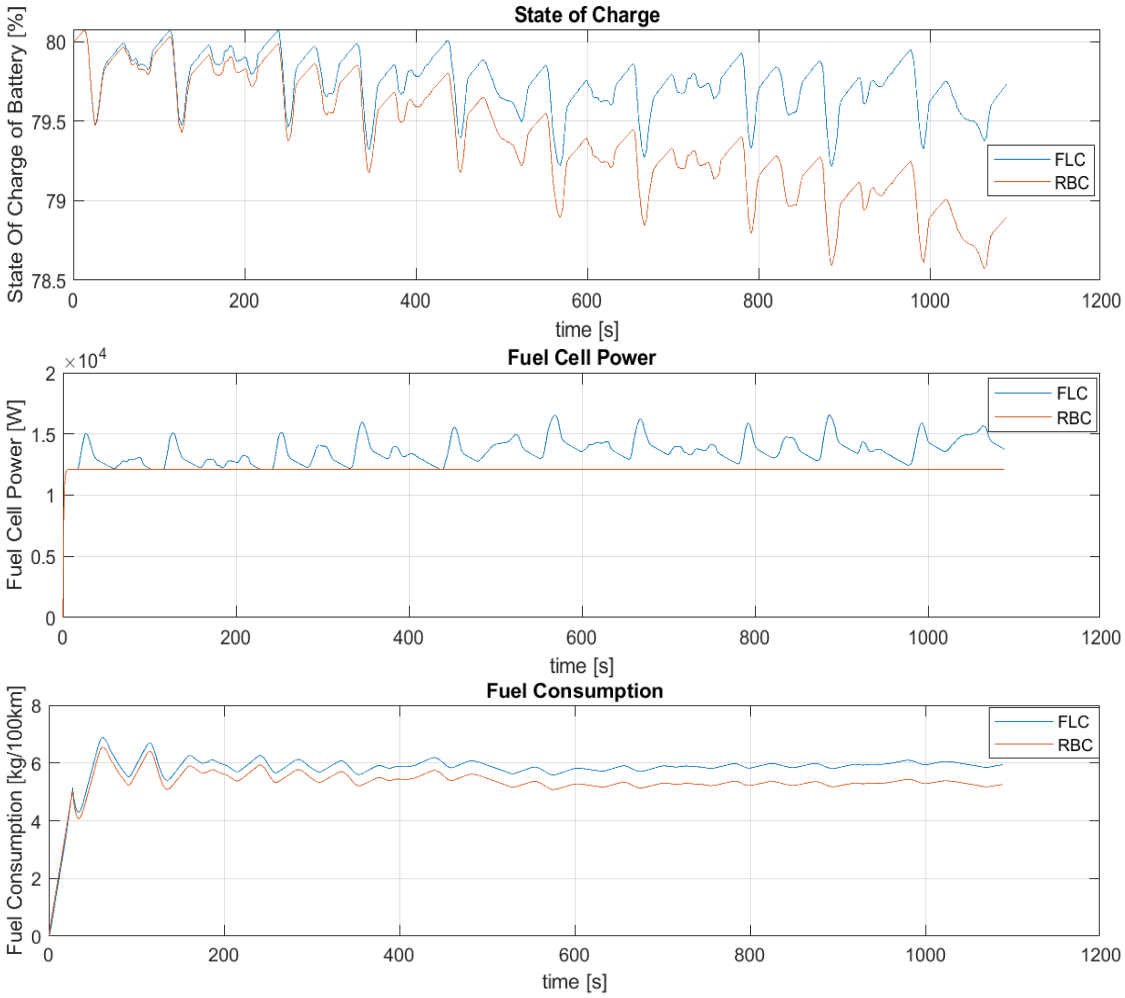

***Figure 50**: Battery SOC, FC Power and FC Fuel consumption comparison for RBC and FLC, with initial SOC = 80%*

Figure 50 show the trend of SOC (State of Charge) and FC (Fuel Cell) power over time for the two different controllers.

It can be noticed that the rule-based strategy is unable to maintain the battery charge level around the desired target, which is 80%, as it shows a decreasing trend instead. The fuel consumption for the FLC is higher, but this can be explained by examining the power output. In fact, the Fuzzy Logic Controller is capable of adjusting the output power to respond to SOC variations by increasing it when necessary. Consequently, it slightly deviates from the operating point of maximum efficiency, thus consuming slightly more hydrogen.

However, it is also important to compare the behavior of the two strategies when the SOC drops below the threshold value, i.e., when the fuel cell controlled by RBC changes operating condition. To achieve this, the initial SOC is set to 74%, slightly below the threshold set at 75%, and the results are presented in Figure 51.

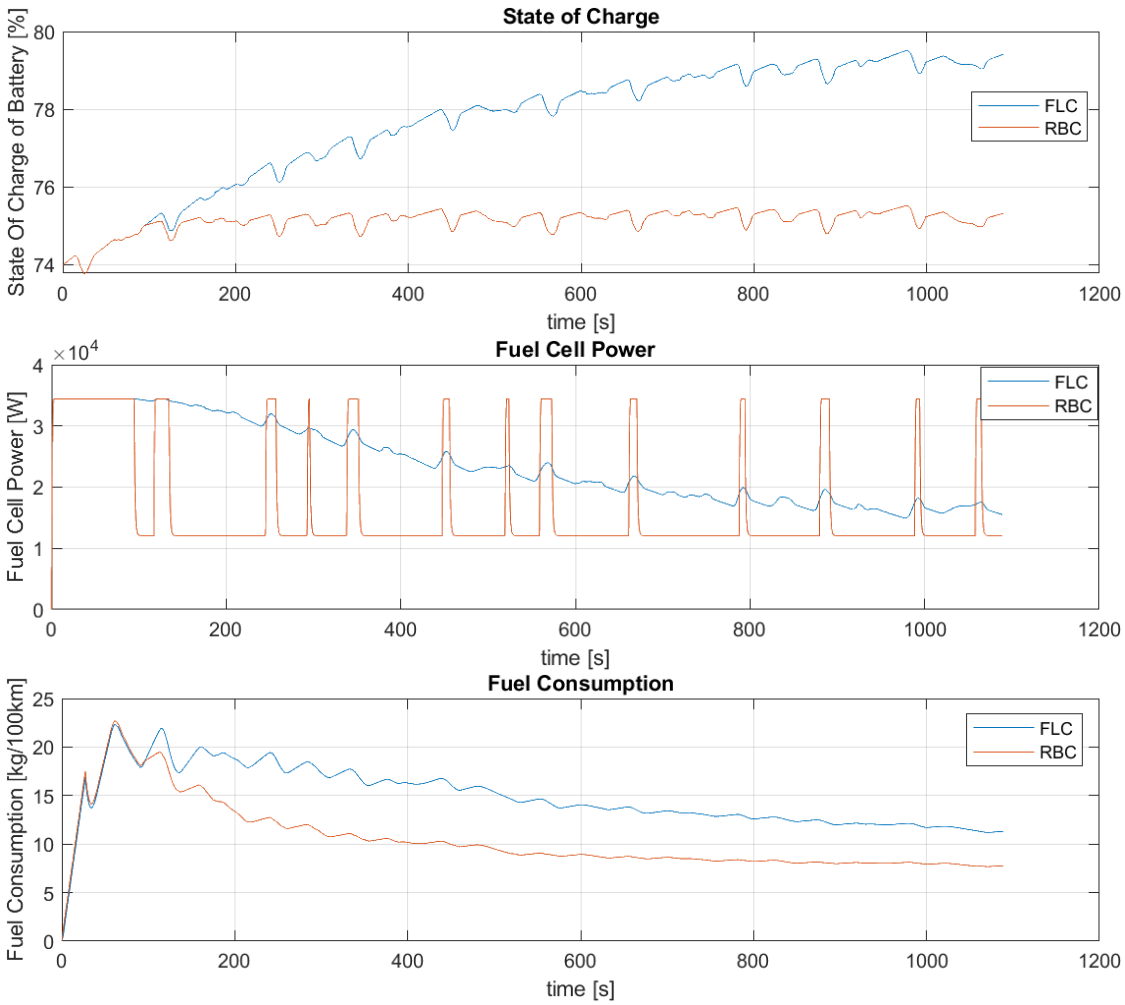

***Figure 51**:Battery SOC, FC Power and FC Fuel consumption comparison for RBC and FLC, with initial SOC = 74%*

In this case, the FCS controlled by the RB (Rule-Based) oscillates between the two working points, creating a highly discontinuous trend for the power. This behavior is to be avoided because, as already reiterated, the Fuel Cell is unable to vary the output power quickly and exhibits performance issues. The fuzzy logic-based strategy, on the other hand, allows for a continuous output power from the FC, which is preferable. Additionally, the SOC value of the battery increases until it closely approaches the target value, while the RBC fails to charge the battery. Once again, the fuel consumption is higher for the FLC, as the FC generates more power during the simulation.

The results obtained are summarized in Table 13, where to enable a qualitative interpretation, the relative difference is calculated.

		Final soc	Soc difference	Fuel consumption
$SOC_{Initial}$=80	**RBC**	78.8	-1.2	5.3
	FLC	79.7	-0.3	5.9
	Relative difference		+75 %	+11.3 %
$SOC_{Initial}$=74	**RBC**	75.3	1.5	7.8
	FLC	79.4	5.4	11.3
	Relative difference		+260 %	+45 %

***Table 13**: Absolute values and relative differences of SOC difference and Fuel consumption between the reference RBC and the FLC*

Considerations on the experienced C-rates and supercapacitor pack inclusion.

The use of a smaller-sized battery has significantly reduced the total mass of the HESS. However, since the new battery has lower capacity, the currents flowing through it generate C-rate values that could be too high (Figure 52).

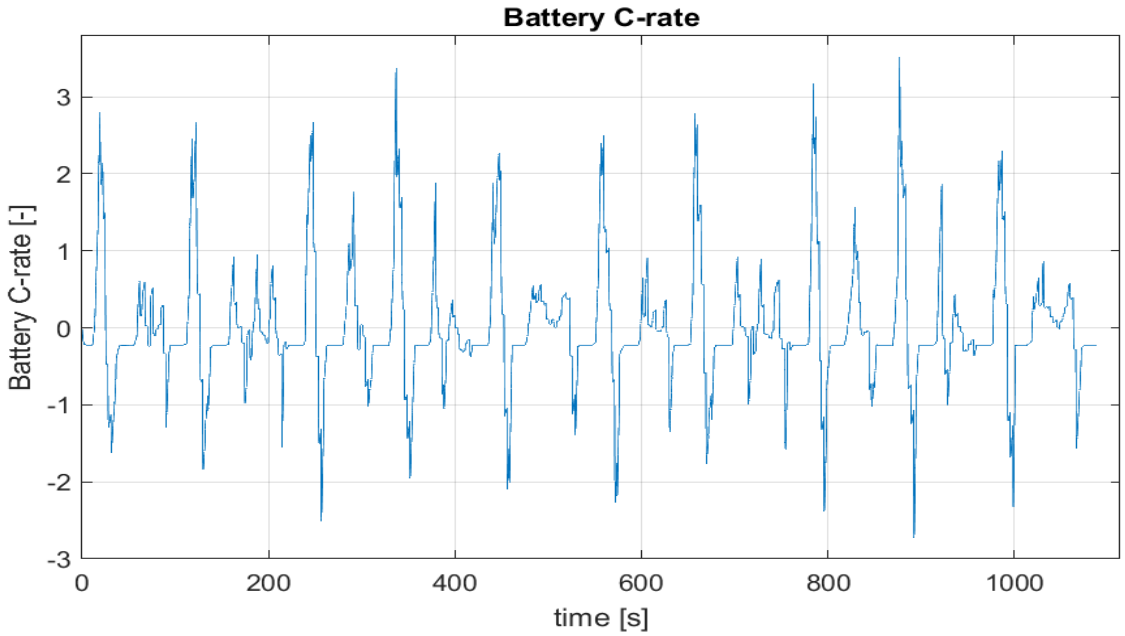

***Figure 52**: Battery C-rate evolution over Manhattan drive cycle for FCHEV*

The simulation conducted on the Manhattan drive cycle reveals how the battery's C-rate peaks exceed 3C several times. Experimenting with such high C-rate values, albeit for short periods, leads to accelerated battery degradation, reducing its lifespan. Addressing this issue could involve increasing the size of the battery, but doing so would partially negate the benefits gained from reducing its mass. Therefore, it was chosen to introduce a supercapacitor SC perfectly identical to the one described in the previous chapter, connected in parallel to the battery and also in series with the fuel cell FC. The SC provides power when demand is high or fluctuates rapidly and, as in the previous case, takes priority over the battery in absorbing power during regenerative braking. The battery, on the other hand, has priority in being continuously recharged by the FCS, and only if its SOC exceeds the predefined threshold the connection between the two components is opened, allowing the FC

system to recharge the SC pack. This simple strategy for regulating the power distribution of the FCS between the battery and SC is summarized in the following pseudocode (Figure 53):

```
READ VoltageSupercapacitor, SOCactual, PowerFuelCell, MaxVoltageSC
SET SocUpperBound= 85%
SETVoltageSCUpperBound= 90% MaxVoltageSC
IF  SOCactual is less than SocUpperBound THEN
      PowerFCtoBattery= PowerFuelCell
      PowerFCtoSC=0
ELSE IF VoltageSupercapacitor is lower than VoltageSCUpperBound THEN
      PowerFCtoBattery= 0
      PowerFCtoSC= PowerFuelCell
ELSE
      PowerFCtoBattery= 0
      PowerFCtoSC= 0
ENF IF
END
```

***Figure 53**: Pseudocode for FC power split*

Figure 54 compares the battery's C-rate trends in the cases with and without the SC.

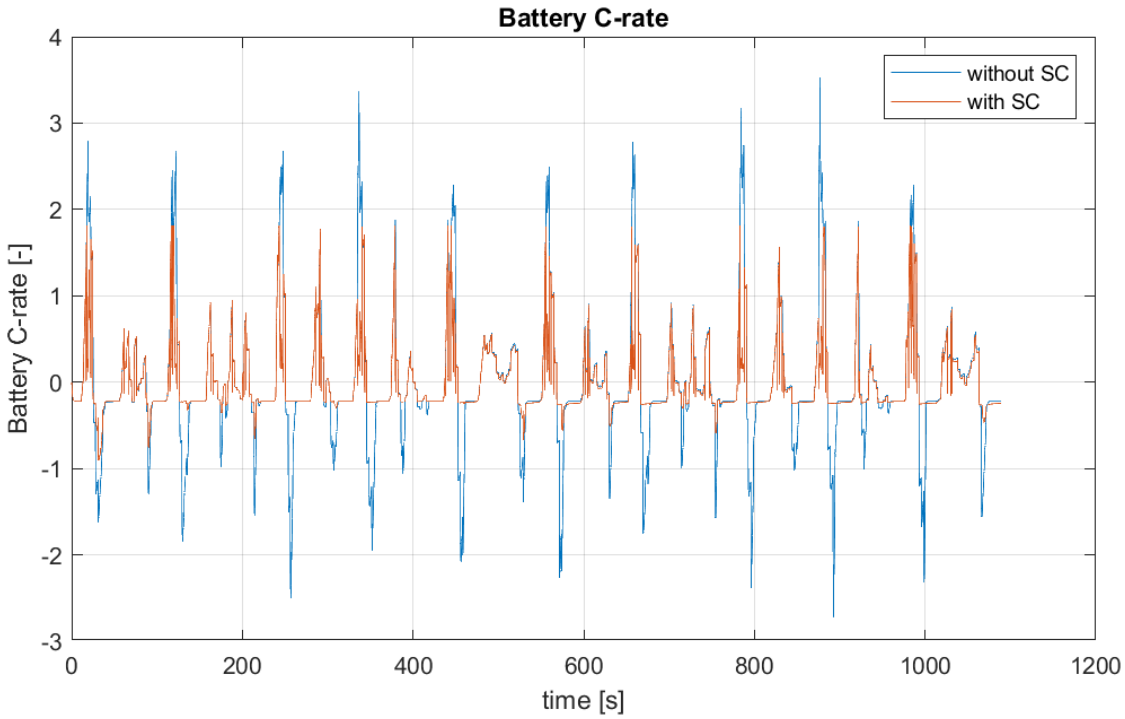

***Figure 54**: Battery C-rate comparison between HESS with and without SC pack*

It can be observed that the presence of the SC significantly reduces the peak C-rate experienced by the battery, which now consistently remains below 2C. Furthermore, by also absorbing power from regenerative braking, it greatly reduces the negative current passing through the battery, thus further limiting the stress it undergoes.
To enable a qualitative comparison, Table 14 shows the RMS values of battery C-rate and their relative differences:

	Without SC	With SC	Relative difference
RMS C-rate	0.76	0.42	-44.7%

***Table 14**: Impact of supercapacitors introduction on battery C-rate values*

Hybrid Energy Storage System Mass Consideration

The mass of the HESS, which includes the Fuel Cell stack as the primary energy source and the Battery and Supercapacitor as power buffers working in synergy, is calculated by summing the individual masses of the components:

$$Mass_{HESS} = Mass_{FCS} + Mass_{Battery} + Mass_{SC} =$$

$$= 145\ kg + 330\ kg + 95\ kg = 570\ kg$$

The difference between the mass of the battery present in the standard production vehicle and that of the HESS developed in this thesis is finally computed and outlined in Table 15:

Baseline Battery mass	HESS mass	Difference	Relative difference
1740 kg	570 kg	1170 kg	-67.2 %

***Table 15**: Mass reduction achieved by HESS*

This result is particularly significant as it translates into a clear reduction in the power required by the powertrain during vehicle use, allowing for better overall energy efficiency. Furthermore, the mass saved by the HESS can be used to accommodate more passengers in the vehicle.

Conclusions

The main topic of this thesis is to explore hybrid electric powertrains for heavy-duty passenger transport vehicles. The primary focus is on the need to extend the battery lifespan and potentially reduce their size to limit the environmental impact associated with their production and disposal.
The benefits obtained through the use of a supercapacitor pack assisting the battery have been analyzed, and several control strategies have been presented. The design of a hybrid electric storage system based on a Fuel Cell Stack as the primary source of energy has been designated as the goal of the work.

After a brief introduction and analysis of the state-of-the-art on hybrid vehicles and control strategies, the first part of this thesis focused on modeling a passenger transport vehicle based on the specifications of the BYD K9 12-meter electric bus. A supercapacitor pack was introduced to work in synergy with the battery and reduce its degradation, leveraging the high-power density characteristic of this component. After selecting the parallel configuration for the two power sources, battery and SC pack, three energy management strategies were presented to determine the optimal power distribution. Following a Design of Experiments to evaluate parameters, a Rule-Based Controller was developed as the control strategy. Subsequently, an adaptive controller for different driving scenarios, also of the RBC type, was developed. The last control strategy presented is based on Fuzzy Logic, allowing the developed controller, to adapt to different scenarios and masses. Simulations conducted in the MATLAB Simulink environment demonstrate that the Root Mean Square value of the battery's C-rate reduces by 32.1% compared to that measured without the presence of SC, indicating a significant extension of the battery life.

The second part of this work aims at the design and modeling of a Fuel Cell Hybrid Electric Vehicle. After presenting the characteristics of this type of vehicle, an analysis of possible architectures was conducted. In the chosen configuration, the FCS is connected in series with a reduced battery, with a total capacity of 100Ah, significantly lower than the capacity of the battery in the baseline vehicle, which is 600Ah, and continuously recharge it, as it is expected to operate in charge-sustaining mode. In this case, two control strategies are presented: in the first one, a Rule-Based Controller mandates the FCS to operate only at two operating points: maximum efficiency or maximum power, depending on the battery SOC. The second strategy, based on fuzzy logic, allows for continuous power output from the FC and is preferred over RBC. It involves the FC operating within the range between the two points of maximum efficiency and maximum power. The described FCHEV significantly reduces the mass of the Hybrid Energy Storage System by having a greatly reduced battery. However, the battery experiences excessively high C-rates, which would lead to rapid degradation. For this reason, a supercapacitor is introduced in parallel with the battery, reducing the experienced C-rates by 44.7%.

The total mass of the HESS is calculated, resulting in a reduction of 67% compared to the mass of the battery in a standard production vehicle.

Next steps in this line of work may involve utilizing the results obtained regarding C-rates to quantify the actual increase in battery lifespan. Additionally, an analysis of the environmental benefits achieved through the use of a reduced-size battery, in terms of greenhouse gas emissions and saved resources, could be conducted. Furthermore, for a more accurate representation, it is possible to include a DC/DC converter loss map. A potential future task involves improving the control strategy developed in this thesis, employing machine learning associated with fuzzy logic to develop an Adaptive Neuro-Fuzzy Inference System (ANFIS) controller. Finally, testing the developed models through hardware-in-the-loop testing after appropriately downscaling the vehicle can lead to acquiring results closer to reality.

Bibliography

[1] T. Swearinger, «Terri Swearinger wins Goldman Prize». Consultato: 1 marzo 2024. [Online]. Disponibile su: https://www.sdearthtimes.com/et0897/et0897s17.html

[2] EU Commision, «'Fit for 55': delivering the EU's 2030 Climate Target on the way to climate neutrality». Consultato: 1 marzo 2024. [Online]. Disponibile su: https://eur-lex.europa.eu/legal-content/EN/TXT/HTML/?uri=CELEX%3A52021DC0550

[3] T. Haas e H. Sander, «Decarbonizing Transport in the European Union: Emission Performance Standards and the Perspectives for a European Green Deal», *Sustainability*, vol. 12, fasc. 20, Art. fasc. 20, gen. 2020, doi: 10.3390/su12208381.

[4] «Trends and developments in electric vehicle markets – Global EV Outlook 2021 – Analysis», IEA. Consultato: 1 marzo 2024. [Online]. Disponibile su: https://www.iea.org/reports/global-ev-outlook-2021/trends-and-developments-in-electric-vehicle-markets

[5] S. Onori, L. Serrao, e G. Rizzoni, *SpringerBriefs in Electrical and Computer Engineering*. 2016. doi: 10.1007/978-1-4471-6781-5.

[6] L. Guzzella e A. Sciarretta, *Vehicle Propulsion Systems: Introduction to Modeling and Optimization*. 2007. doi: 10.1007/978-3-642-35913-2.

[7] J. Shailendra e K. Lalit, *31: Fundamentals of Power Electronics Controlled Electric Propulsion - Power Electronics Handbook, 4th Edition [Book]*. Consultato: 1 marzo 2024. [Online]. Disponibile su: https://www.oreilly.com/library/view/power-electronics-handbook/9780128114087/B9780128114070000350.xhtml

[8] J. M. Miller, *Propulsion Systems for Hybrid Vehicles*. IET, 2004.

[9] A. Panday e H. Bansal, «Fuel Efficiency Optimization of Input-Split Hybrid Electric Vehicle using DIRECT Algorithm», presentato al 9th International Conference on Industrial and Information Systems, ICIIS 2014, dic. 2014. doi: 10.1109/ICIINFS.2014.7036640.

[10] G. Rizzoni e H. Peng, «Hybrid and Electrified Vehicles», *Mech. Eng.*, vol. 135, fasc. 03, pp. S10–S17, mar. 2013, doi: 10.1115/1.2013-MAR-5.

[11] M. Kamran, «Chapter 10 - Electric vehicles and smart grids», 2022, pp. 431–460. doi: 10.1016/B978-0-323-99560-3.00002-8.

[12] S. M. Bhagavathy, H. Budnitz, T. Schwanen, e M. McCulloch, «Impact of Charging Rates on Electric Vehicle Battery Life», *Findings*, mar. 2021, doi: 10.32866/001c.21459.

[13] E. Emilsson e L. Dahllöf, *Lithium-Ion Vehicle Battery Production Status 2019 on Energy Use, CO 2 Emissions, Use of Metals, Products Environmental Footprint, and Recycling*. 2019. doi: 10.13140/RG.2.2.29735.70562.

[14] X. Sun, Z. Li, X. Wang, e C. Li, «Technology Development of Electric Vehicles: A Review», *Energies*, vol. 13, fasc. 1, p. 90, dic. 2019, doi: 10.3390/en13010090.

[15] E. Mulholland, J. Miller, C. Braun, A. Sen, P.-L. Ragon, e F. Rodriguez, *The CO2 standards required for trucks and buses for Europe to meet its climate targets*. 2022.

[16] J. Jia, Y. Wang, Q. Li, Y. T. Cham, e M. Han, «Modeling and Dynamic Characteristic Simulation of a Proton Exchange Membrane Fuel Cell», *Energy Convers. IEEE Trans. On*, vol. 24, pp. 283–291, apr. 2009, doi: 10.1109/TEC.2008.2011837.

[17] «Production of hydrogen - U.S. Energy Information Administration (EIA)». Consultato: 1 marzo 2024. [Online]. Disponibile su: https://www.eia.gov/energyexplained/hydrogen/production-of-hydrogen.php

[18] K. Lakshmi e B. Vedhanarayanan, «High-Performance Supercapacitors: A Comprehensive Review on Paradigm Shift of Conventional Energy Storage Devices», *Batteries*, vol. 9, p. 202, mar. 2023, doi: 10.3390/batteries9040202.

[19] J. Cao e A. Emadi, «A New Battery/UltraCapacitor Hybrid Energy Storage System for Electric, Hybrid, and Plug-In Hybrid Electric Vehicles», *Power Electron. IEEE Trans. On*, vol. 27, pp. 122–132, feb. 2012, doi: 10.1109/TPEL.2011.2151206.

[20] L. Kouchachvili, W. Yaïci, e E. Entchev, «Hybrid battery/supercapacitor energy storage system for the electric vehicles», *J. Power Sources*, vol. 374, pp. 237–248, gen. 2018, doi: 10.1016/j.jpowsour.2017.11.040.

[21] C. Xiang, Y. Wang, S. Hu, e W. Wang, «A New Topology and Control Strategy for a Hybrid Battery-Ultracapacitor Energy Storage System», *Energies*, vol. 7, pp. 2874–2896, apr. 2014, doi: 10.3390/en7052874.

[22] S. Onori, L. Serrao, e G. Rizzoni, *SpringerBriefs in Electrical and Computer Engineering*. 2016. doi: 10.1007/978-1-4471-6781-5.

[23] A. Sciarretta e L. Guzzella, «Control of hybrid electric vehicles», *Control Syst. IEEE*, vol. 27, pp. 60–70, mag. 2007, doi: 10.1109/MCS.2007.338280.

[24] T. Hofman, M. Steinbuch, D. RM, e A. Serrarens, «Rule-based energy management strategies for hybrid vehicle drivetrains: A fundamental approach in reducing computation time», *Brain Res. - BRAIN RES*, gen. 2006.

[25] A. Rubaai, «35 - Fuzzy Logic in Electric Drives», in *Power Electronics Handbook (Second Edition)*, M. H. Rashid, A c. di, in Engineering. , Burlington: Academic Press, 2007, pp. 999–1013. doi: 10.1016/B978-012088479-7/50053-5.

[26] T. Bharathi e M. Kumar, «A STUDY ON FUZZY LOGIC CONTROLLER», giu. 2016.

[27] van Leekwijck, W., W. van Leekwijck, e E. E. Kerre, «Defuzzification: criteria and classification», *Fuzzy Sets Syst.*, vol. 108, fasc. 2, pp. 159–178, 1999, doi: 10.1016/S0165-0114(97)00337-0.

[28] T. Mitsuishi, «Definition of Centroid Method as Defuzzification», *Formaliz. Math.*, vol. 30, fasc. 2, pp. 125–134, lug. 2022.

[29] L. Serrao, S. Onori, e G. Rizzoni, «A Comparative Analysis of Energy Management Strategies for Hybrid Electric Vehicles», *J. Dyn. Syst. Meas. Control*, vol. 133, p. 031012, mag. 2011, doi: 10.1115/1.4003267.

[30] Z. Fu, Z. Li, P. Si, e F. Tao, «A hierarchical energy management strategy for fuel cell/battery/supercapacitor hybrid electric vehicles», *Int. J. Hydrog. Energy*, vol. 44, fasc. 39, pp. 22146–22159, ago. 2019, doi: 10.1016/j.ijhydene.2019.06.158.

[31] O. El Ganaoui-Mourlan, E. H. Miliani, D. Carlos Da Silva, M. Couillandeau, C. Gonod, e G. Miller, «Design of a Flexible Hybrid Powertrain Using a 48 V-Battery and a Supercapacitor for Ultra-Light Urban Vehicles», presentato al SAE International, 2020. [Online]. Disponibile su: https://doi.org/10.4271/2020-01-0445

[32] I. Shafikhani, C. Sundström, J. Åslund, e E. Frisk, «MPC-based energy management system design for a series HEV with battery life optimization», in

2021 European Control Conference (ECC), giu. 2021, pp. 2591–2596. doi: 10.23919/ECC54610.2021.9655224.

[33] P. Pettersson, B. Jacobson, F. Bruzelius, P. Johannesson, e L. Fast, «Intrinsic differences between backward and forward vehicle simulation models», *IFAC-Pap.*, vol. 53, pp. 14292–14299, gen. 2020, doi: 10.1016/j.ifacol.2020.12.1368.

[34] J. Peng, J. Jiang, F. Ding, e H. Tan, «Development of Driving Cycle Construction for Hybrid Electric Bus: A Case Study in Zhengzhou, China», *Sustainability*, vol. 12, fasc. 17, Art. fasc. 17, gen. 2020, doi: 10.3390/su12177188.

[35] S. Motapon, L.-A. Dessaint, e K. Al-Haddad, «A Comparative Study of Energy Management Schemes for a Fuel-Cell Hybrid Emergency Power System of More-Electric Aircraft», *Ind. Electron. IEEE Trans. On*, vol. 61, pp. 1320–1334, mar. 2014, doi: 10.1109/TIE.2013.2257152.

[36] J. Zubieta e R. Bonert, «Characterization of Double-Layer Capacitors for Power Electronics Applications», *Ind. Appl. IEEE Trans. On*, vol. 36, pp. 199–205, feb. 2000, doi: 10.1109/28.821816.

[37] C. H. Wu, Y. H. Hung, e C.-W. Hong, «On-line supercapacitor dynamic models for energy conversion and management», *Energy Convers. Manag.*, vol. 53, pp. 337–345, gen. 2012, doi: 10.1016/j.enconman.2011.01.018.

[38] S. Pezzolato, «Modeling and model validation of supercapacitors for real-time simulations», Tesi di laurea, 2020. Consultato: 1 marzo 2024. [Online]. Disponibile su: https://amslaurea.unibo.it/20083/

[39] A. Foelske, O. BARBIERI, M. HAHN, e R. Kötz, «An X-Ray Photoelectron Spectroscopy Study of Hydrous Ruthenium Oxide Powders with Various Water Contents for Supercapacitors», *Electrochem. Solid-State Lett.*, vol. 9, pp. A268–A272, giu. 2006, doi: 10.1149/1.2188078.

[40] FuelCellsWorks, «Horizon Automotive PEM Fuel Cells To Set 300kW Benchmark - FuelCellsWorks». Consultato: 11 marzo 2024. [Online]. Disponibile su: https://fuelcellsworks.com/news/horizon-automotive-pem-fuel-cells-to-set-300kw-benchmark/

[41] J. Bauman e M. Kazerani, «A Comparative Study of Fuel-Cell–Battery, Fuel-Cell–Ultracapacitor, and Fuel-Cell–Battery–Ultracapacitor Vehicles», *Veh. Technol. IEEE Trans. On*, vol. 57, pp. 760–769, apr. 2008, doi: 10.1109/TVT.2007.906379.